University of South-Eastern Norway
Faculty of Technology, Natural Sciences and Maritime Studies
—
Doctoral dissertation no. 152
2023

Yelzhas Zhaksylyk

Inductive impedance matching network for Magnetic Resonant Wireless Power Transmission

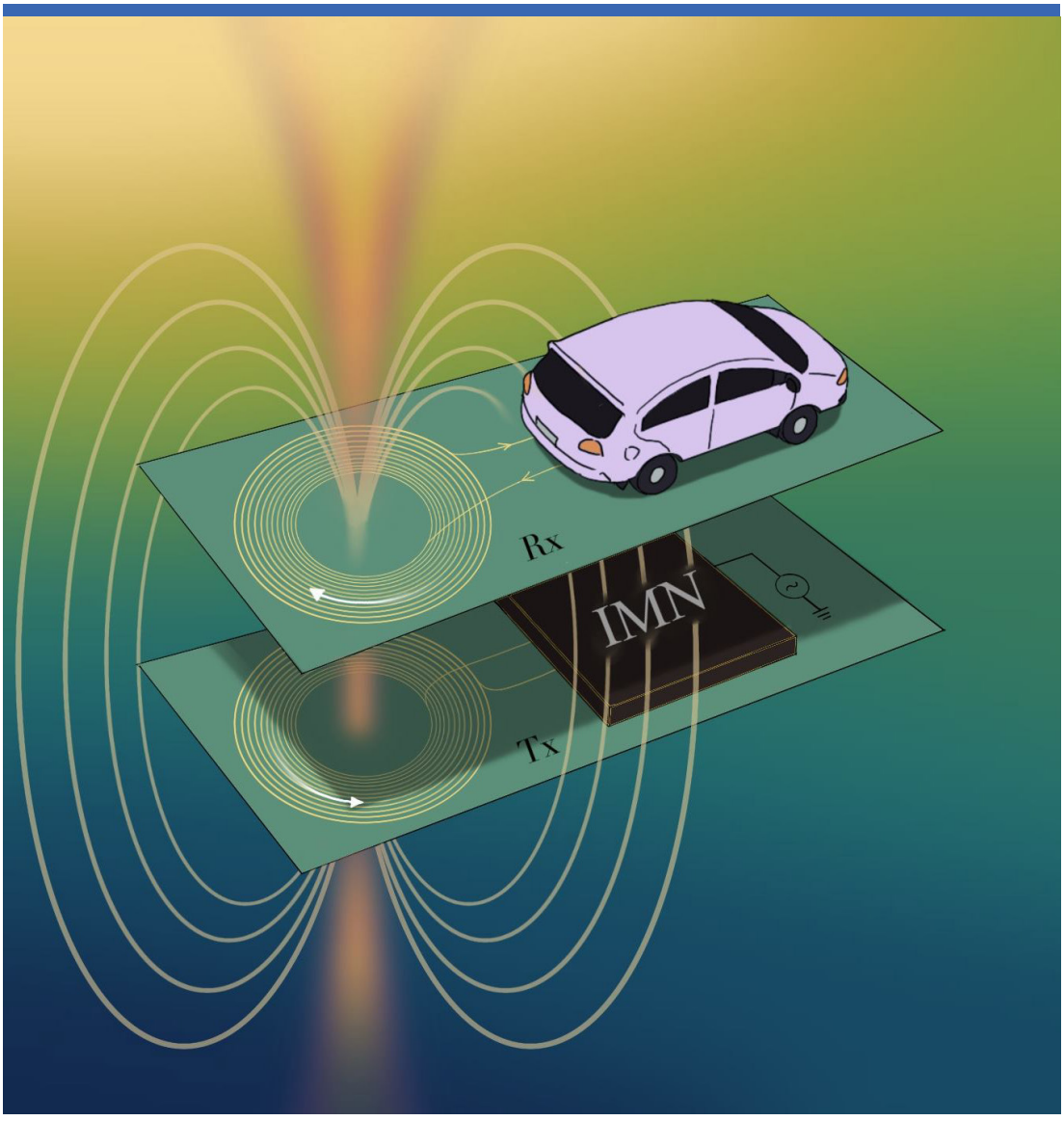

Yelzhas Zhaksylyk

Inductive impedance matching network for Magnetic Resonant Wireless Power Transmission

A PhD dissertation in
Applied micro- and nanosystems

© Yelzhas Zhaksylyk, 2023

Faculty of Technology, Natural Sciences and Maritime Studies
University of South-Eastern Norway
Horten, 2023

Doctoral dissertations at the University of South-Eastern Norway no. 152
ISSN 2535-5244 (print)
ISSN 2535-5252 (online)

ISBN 978-82-7206-737-2 (print)
ISBN 978-82-7206-738-9 (online)

This publication is licensed with a Creative Commons license. You may copy and redistribute the material in any medium or format. You must give appropriate credit, provide a link to the license, and indicate if changes were made. Complete license terms at https://creativecommons.org/licenses/by-nc-sa/4.0/deed.en

Print: University of South-Eastern Norway

Acknowledgements

I wish my sincere gratitude to my principal supervisor Prof. Mehdi Azadmehr and co-supervisors, Profs. Ulrik Hanke and Einar Halvorsen for their invaluable counsel, thoughtful feedback, and great support during my PhD journey.

I am also thankful to all professors and staff at the department of MicroSystems for their help in organizing laboratory setup, managing administration issues, and for all the considerate guidance. Special thanks to my colleague Oleksandr Dobroliubov for interesting coffee breaks.

Finally, I want to express gratitude to my family and wife, Assel, for always being there for me. Their support and love during these three years helped me focus on my research and continue my career path.

Abstract

Inductive wireless power transfer is getting more and more attention as the demand for mobile electronic devices grows. There are already well-functioning wireless charging systems for smartphones, tablets, and electric toothbrushes. The main disadvantage of these systems is a degradation of power transfer efficiency due to misalignment and distance variation between the charging station and the devices. This degradation limits the mobility of devices due to impedance mismatch in the system and can be compensated by using proper impedance matching techniques.

Impedance matching (IM) is a technique used to optimize the power transfer from a source to a load, also applicable in wireless power transfer (WPT) systems. There are two main IM approaches, namely capacitive and inductive matching. Capacitive impedance matching network (IMN) is the main approach used in most WPT systems, and it is widely discussed in the literature. Inductive is less common, and therefore, only a few inductive matching techniques have been reported. This PhD project aims to compare these two IMNs for use in WPT systems and, in addition, proposes new methods for inductive impedance matching.

Although the capacitive and inductive IMN are fundamentally different, we developed a method for comparing these and concluded that the same level of matching could be achieved. This conclusion is proved analytically using circuit theory, simulation, and visualized on Smith charts.

This thesis proposes two new methods of tunable inductive IMN for use in magnetic resonance WPT. These methods offer an efficient driving and tuning of a resonating coil with a simple and compact design for easy and low-cost production. The study also compares the proposed approaches to the existing alternatives, such as using high-quality variable capacitors (varactors) for actively tuning the system for optimal power transfer.

List of Publications

Articles i, ii, iv and v are omitted from online publication

- **Article I**
  Y. Zhaksylyk and M. Azadmehr, "Comparative Analysis of Inductive and Capacitive Feeding of Magnetic Resonance Wireless Power Transfer," 2018 IEEE PELS Workshop on Emerging Technologies: Wireless Power Transfer (Wow), Montréal, QC, 2018, pp. 1-5, doi: 10.1109/WoW.2018.8450891.

- **Article II**
  Y. Zhaksylyk, U. Hanke and M. Azadmehr, "Design of a switchable driving coil for Magnetic Resonance Wireless Power Transfer," 2019 IEEE PELS Workshop on Emerging Technologies: Wireless Power Transfer (WoW), London, United Kingdom, 2019, pp. 249-252, doi: 10.1109/WoW45936.2019.9030674.

- **Article III**
  Y. Zhaksylyk, E. Halvorsen, U. Hanke, and M. Azadmehr, "Analysis of Fundamental Differences between Capacitive and Inductive Impedance Matching for Inductive Wireless Power Transfer", Electronics 2020, 9, 476, doi: 10.3390/electronics9030476

- **Article IV**
  Y. Zhaksylyk, U. Hanke and M. Azadmehr, "Impedance Matching using Interspiraled Coils for Wireless Power Transfer," 2020 IEEE PELS Workshop on Emerging Technologies: Wireless Power Transfer (WoW), Seoul, Korea, 2020, pp. 346-349, doi: 10.1109/WoW47795.2020.9291325.

- **Article V**
  Y. Zhaksylyk, U. Hanke, and M. Azadmehr, "Single-side interspiraled inductive impedance matching for Magnetic Resonance Wireless Power Transfer", is submitted to IEEE Transactions on Circuits and Systems I: Regular Papers.

- **Patent**
  Y. Zhaksylyk and M. Azadmehr, patent "A Coil structure for impedance matching in a wireless power transfer system", filed

Co-Author of the following publications:

These articles were not included in the thesis.

- **Article VII**
  P. Le Bihan, Y. Zhaksylyk, P.D.H. Re, S.K. Podilchak, M. García-Vigueras, and G. Goussetis, "Dual-circularly polarized patch antenna using simple isolation techniques and its array application", IET Conference Proceedings, 2018, p. 776 (5 pp.)-776 (5 pp.), doi: 10.1049/cp.2018.1135

- **Article VIII**
  P. Le Bihan, Y. Zhaksylyk et al., "Dual-Polarized Aperture-Coupled Patch Antennas With Application to Retrodirective and Monopulse Arrays," in IEEE Access, vol. 8, pp. 7549-7557, 2020, doi: 10.1109/ACCESS.2019.2961601.

List of Figures

Contents

1 Introduction

Nowadays, wireless technology has spread widely because of the increasing demand for mobility and accessibility of electronic devices. Technologies such as WiFi and Bluetooth offer good solutions for communication, however, the main challenge is still the access to power. Today, all power is delivered by either batteries or cables, which are the main limitations in the mobility of devices. Research on wireless power transfer is seeking to solve this issue and offer fully wireless devices.

At the moment, wireless power transfer (WPT) is a primary area of research and development in many universities and industries all around the world. Companies such as WiTricity, Braun, Thales, and Samsung have already implemented WPT in their products, and large national agencies such as NASA and the Japanese Space Agency (JAXA) have extensive research in the field [1]. Many concepts of wireless power transfer for various applications and areas such as in homes, space, and industry are presented. An example of a concept for a wireless power system in a home is illustrated in Fig. 1.1, where one power transmitting device can power and charge all the necessary electronics in a room.

Figure 1.1: Concept of wireless power transfer for home appliances.

1.1 Background

The concept of wireless power transfer is not new, it was proposed as early as in the late 1800s. The first experiment was completed by H.R. Hertz

in 1888, where he successfully transferred power between two oscillators during his research on Maxwell's equations [2]. The experiment proved both the existence of electromagnetic radiation and Maxwell's equations. The first patent of WPT describing a wireless electric lighting system at high frequency was filed in 1891 by Nicola Tesla, who is also referred to as the father of the WPT [3]. In this patent, electrical transformers are used to light single terminal carbon lamps with only one supplying wire. In the following years, Tesla had completed several experiments and patented numerous inventions, such as the famous 'Tesla Coil'. Wardenclyffe or Tesla Tower is among the list of widely spoken experiments in the wireless community built in New York in 1901-1902 to power the world with wireless electricity. His idea of the 'World Wireless System' is based on transmitting electricity at the resonance frequency of Earth. However, the experiment was abandoned due to financial issues.

Other methods for wireless power transmission have also emerged in the last decades, such as acoustic, Microwave, capacitive, etc. They are presented in Fig. 1.2.

Piezoelectric transducers are capable of transmitting and receiving power through acoustic vibratory signals [4], as shown Fig. 1.2(a). The main advantage of piezoelectric acoustic power transfer is low attenuation in different mediums such as water, tissue, etc. This property makes them ideal for biomedical implants and sub-sea applications.

Coherent laser beams can transfer a very high amount of energy, which is an efficient approach to transmit power point-to-point. NASA was able to charge an unmanned aircraft by this mechanism in 2003, where the receiver part was made of an infrared photovoltaic cell, Fig. 1.2(b). NASA is planning to charge their satellites using laser beam since other mechanisms are not applicable in such harsh environment [5].

Another approach for point-to-point power transfer is Microwave, which can be used for transferring high power for long distances [6]. There is an entire field of research for the study of rectennas, for receiving energy from microwaves [7], Fig. 1.2(c). However, this technology requires expensive alignment and tracking systems to maintain a point-to-point connection between transmitter and receiver.

RF broadcasting can be used for omnidirectional power transfer where the system does not require complicated tracking software. This technique has a large coverage area, but the power level drops significantly over the distance due to spreading, and hence the power at the receiver is much smaller than transmitted [8].

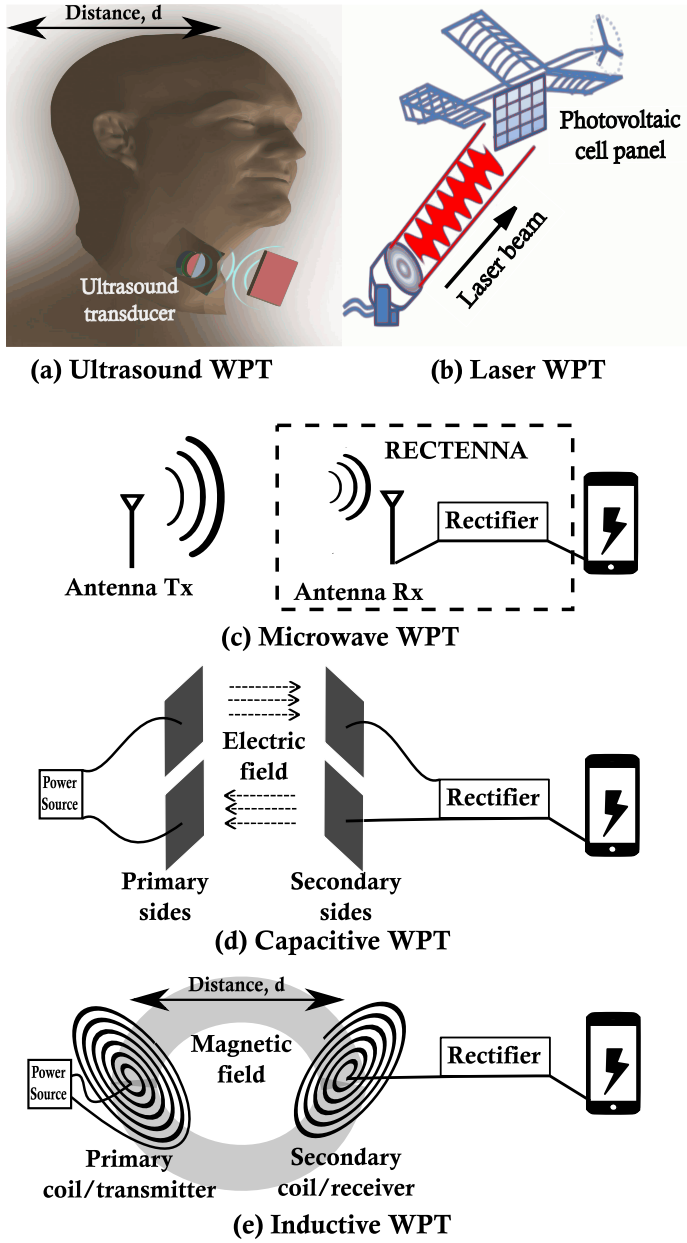

Figure 1.2: Most common methods of wireless power transfer.

Capacitive power transfer (CPT) uses high-frequency electric fields (EF) for the effective transmission of electric power. The advantages of CPT are small eddy-current loss, low cost, compact design, and insensitivity to misalignment [9], Fig. 1.2(d). The main drawbacks of CPT are the limited distance of operation and high voltage requirement, which may cause safety issues.

The most conventional method today is based on inductive coupling, which works by utilizing magnetic induction between two coils. This method is limited only to close ranges [10, 11], Fig. 1.2(e) i.e. in the near field. The working principle resembles a transformer, where alternating current on the transmitter (primary) coil generates an alternating magnetic field, which induces AC current on the receiver (secondary) coil. The AC current at the receiver side is then rectified and delivered to the load. Magnetic resonant WPT is based on this inductive WPT, which exploits the phenomena of resonance. It utilizes high-quality resonators to achieve efficient power transmission for several dozens of centimeters at a given resonance frequency [12, 13].

1.2 Application and challenges of inductive wireless charging

For daily-life applications, magnetic resonant inductive WPT is the favorite as it offers the highest power transfer efficiency (PTE) among the alternatives mentioned in the previous section. Various products such as electric toothbrushes and mobile phone chargers using this technique are already commercially available. Inductive wireless power transmission provides two advantages compared to others: transfer of high power and low operation frequency, making it less hazardous to the human body [14]. The main limitation with the inductive WPT is the mobility as the sender and receiver need to be aligned and placed close to each other, normally less than a few cm. Magnetic resonant (MR) wireless power transfer (WPT), an inductive technique operated at the resonance frequency of transmitter and receiver systems, solves this problem and provides high power efficiency at a reasonable distance of power transfer (up to 2m) [12]. However, a considerable challenge of the resonant technique is the drop in power transfer efficiency (PTE) due to the change in distance between resonators at the operation frequency within the allowed Industrial, Scientific, and Medical (ISM) bands [15].

In addition to the change in distance, the efficiency of magnetic

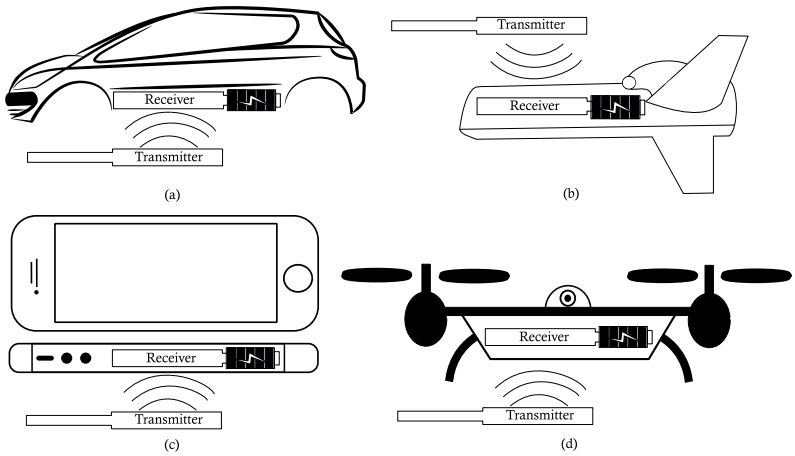

Figure 1.3: Potential wireless charging stations with compensation system for distance changes: (a) electric vehicle charging station; (b) autonomous submarine charging station; (c) smartphone charging setup; (d) drone charging system.

resonance wireless power transfer is also highly sensitive to impedance changes in the system due to misalignment between coils and load variation. Most common applications that will struggle from the misalignment and variation in the distance are shown in Fig. 1.3. Fig. 1.3(a) is an electric vehicle (EV) wireless charging system. Current solutions of EV charging offer static charging stations on parking slots, where a car has to be parked exactly on a given spot, which can be inconvenient. Through adaptive compensation circuitry, this problem may, however, be solved. Adaptive compensation circuits also enable dynamic wireless charging, i.e., power exchange between the car and the transmitter while the car is moving [16–18].

Fig. 1.3(b) shows an autonomous electric UAV charging station, where a transmitter system can be placed on the dock. The charging process happens when the UAV requires charging and rises to the dock station. The sea is an unpredictable environment that makes the charging challenging, and there are no good solutions today. Fig. 1.3(c) presents a commercially available product - a smartphone charging pad. However, similar to EV charging, it requires precise placement of the phone on the charging pad, and misalignment decreases the efficiency or even stops the charging process. Finally, Fig. 1.3(d) is a drone charging station. Similar to the electric UAV charging system, it is still on research-level since the system has to be insensitive towards misalignment and load changes.

1.3 Motivation of this PhD work

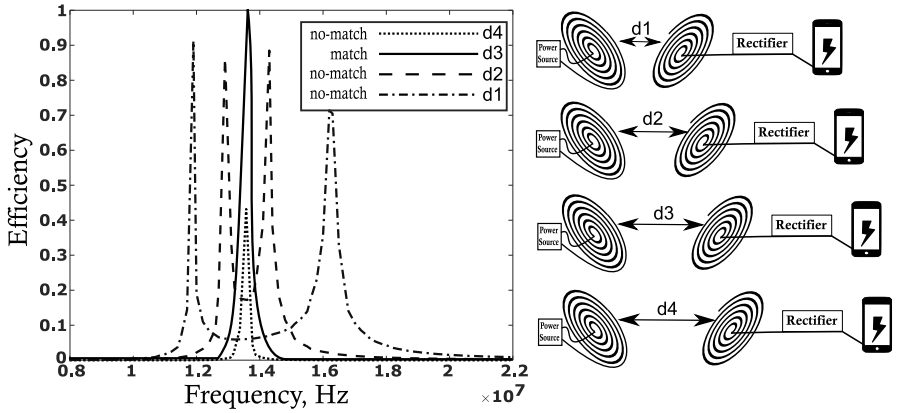

Figure 1.4: Efficiency of inductive power transfer versus frequency and distance.

The most important reason for the drop in PTE, as discussed in the previous section, is the impedance mismatch [19] due to the change in distance between coils. Fig. 1.4 shows the system response for four different distances. In this figure, the system is matched for maximum efficiency at the distance $d3$ for a predefined frequency of 13.56 MHz. At shorter distances, referred to as the over-coupled region, marked as $d1$ and $d2$ in the figure, there is a frequency splitting phenomenon (will be discussed in section 2.1) which results in a drop of the PTE at the predefined operation frequency. At a longer distance, also referred to as the under-coupled region shown as $d4$ in the figure, the PTE will drop due to the weakening of a magnetic field and impedance mismatch.

The efficiency at the over-coupled region can be improved by two methods, either by adaptive frequency tuning or impedance matching. Adaptive frequency tuning, as its name suggests, is a technique based on tuning the operating frequency for the desired performance of the system, i.e., for compensation of the mismatch in the over coupled region [20]. In Fig. 1.4, the operation frequency should be set to 12 MHz at a distance $d1$ to achieve the best PTE and adjusted to 13.56 MHz at the matched distance $d3$. There are two main disadvantages to this technique. The first one is that the adaptive frequency tuning is impractical at further distances than the matched distance $d3$ as there is not enough magnetic flux to offer maximum efficiency. The second one is the ISM bands limit the frequency of operation.

A more feasible method is to use impedance matching networks (IMNs) to compensate for the mismatches, instead of frequency tuning.

1.4 Impedance matching network for WPT

In order to solve efficiency instabilities, an effective impedance matching network (IMN) is required. Different methods of IMNs are developed during the last decades. Moreover, IMN can be used to transfer power to multiple devices by using only a single transmitter [15].

A schematic model of an inductive WPT with IMNs is shown in Fig. 1.5. A power source drives the transmitter coil L_T through IMN_{TX}. The coil L_T is magnetically coupled to a receiver coil L_R with a distance d between the coils. Receiver coil L_R is connected through the IMN_{RX} to the load, which in this case is a phone.

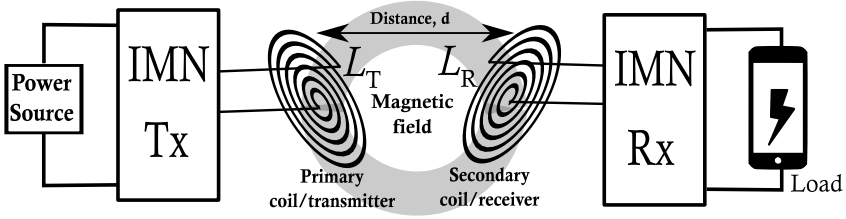

Figure 1.5: Schematic view of inductive WPT system with IMN at transmitter and receiver sides.

The first usage of impedance matching can be seen as early as in the patent by Nikola Tesla from 1897 [3]. The patent describes a high-power transformer designed for the high-frequency application, shown in Fig. 1.6. The generator G supplies coil C, which magnetically couples to coil B as a step-up transformer. Coil B has two connections - one to the ground and one to coil B'. Finally, the coils B' and C' create a step-down transformer and deliver the electricity to load H. As the coils C and B are symmetrical to the coils C' and B', the system reminds of a four-coil inductive wireless power transfer system.

A four-coil inductive WPT system presented by the MIT group in 2007 [12] gained popularity for highly resonant WPT systems for medium distances [21–23]. A schematic model of the system is shown in Fig. 1.7. The system consists of two high-Q resonating transmitter/receiver coils

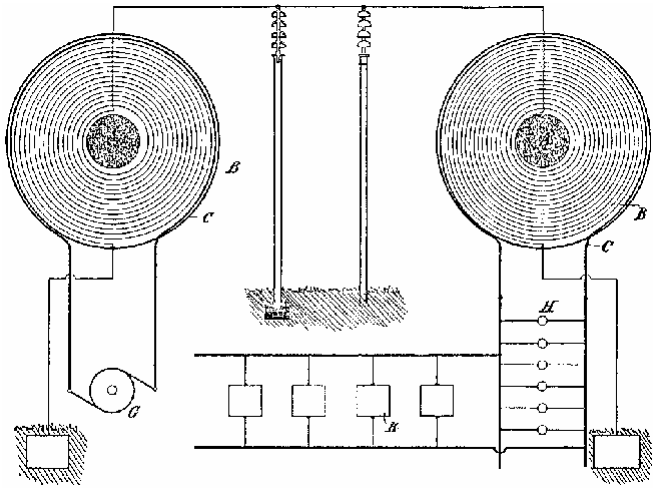

Figure 1.6: Tesla patent issued in 1897: Electrical transformer [3].

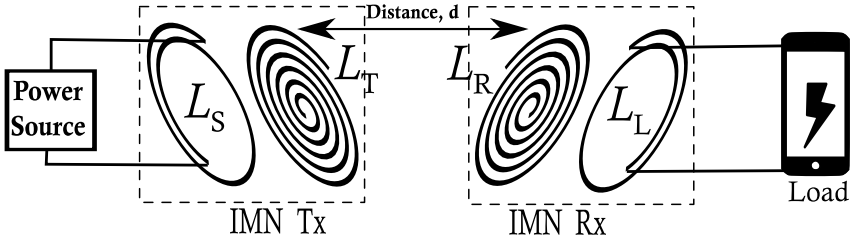

Figure 1.7: Equivalent model of WPT system with multiple coils by MIT.

L_T/L_R, where transmitter coil L_T is driven by a low-Q coil L_S connected to the alternating power source, Fig. 1.7. The load is also connected to a low-Q coil L_L. The magnetic coupling between high-Q and low-Q coils can be considered as parts of a matching network, where the tuning of the impedance can be achieved by changing the couplings between them. In our study, this method is implemented and referred to as inductive matching.

In high-frequency applications, inductive matching is bulky and adds ohmic loss in the system [24]. Hence, capacitive IMNs are widely used for WPT systems. The capacitive method uses tuning capacitors to tune the system to the resonance frequency, normally by using a predefined capacitor sequence or varactors [25, 26]. There is a variety of adaptive frequency tuning systems where L, T and Π-type capacitive impedance matching networks are used [27, 28].

Capacitors can also be connected in series and parallel to the coils

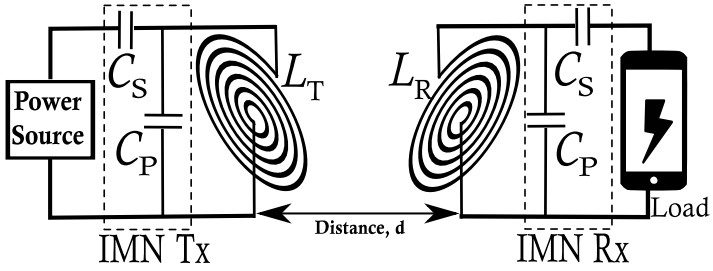

Figure 1.8: Equivalent model of WPT system with capacitive IMNs with series-parallel(SP) compensation or parallel–series (PS) compensation.

to achieve IMN, i.e., series-parallel (SP) compensation or parallel–series (PS) compensation IMNs. An equivalent model of the WPT system with capacitive compensation methods is shown in Fig. 1.8. Impedance changes can be compensated by varying values of capacitors C_S and C_P in the IMN both at the transmitter and the receiver. Global standardizations of Alliance for Wireless Power Consortium (A4WP) and Wireless Power Consortium (WPC) recommend SP and PS IMNs [29, 30]. Moreover, there are many research studies on usage of SP and PS IMNs [27–32]. However, there is limited information on the performance of IMNs with different combinations such as SP and SP networks, SP-PS, PS-SP, and PS-PS.

In this thesis, we compare the presented capacitive and inductive techniques in terms of performance and propose new types of inductive matching based on switching tunable coils.

1.5 Thesis outline

The thesis is divided into four main chapters. The first chapter focuses on the background of wireless power transfer and the motivation of this PhD project. There is also a discussion on the development of impedance matching networks for inductive WPT systems, which is also the focus of the thesis.

The second chapter gives an overview of the state of the art impedance matching networks (IMNs) for inductive WPT systems. A comparison of the two popular techniques of compensation circuitry, namely inductive and capacitive, is also presented. The comparison is performed using the Smith chart, the results of this work are published in conference and journal articles: Article I and Article III.

After the comparative analysis of IMNs, a new method of IMN using switchable inductors is proposed, which is discussed in Chapter 3. The initial design of the multi-coil inductive IMN detailed in the thesis was first documented in a conference paper - Article II. This is followed by an introduction of the second design of an inductive IMN based on interspiraled coils, which is published in a conference paper - Article IV. This paper is extended into a journal article - Article V, where single-side impedance matching using interspiraled coils is studied. Finally, the chapter ends with some additional circuit analysis and simulation results on two-side impedance matching in the WPT system using interspiraled coils, which are not published.

The final chapter concludes the thesis. An overview of the research impact is discussed and followed by suggestions for future work on the topic.

2 Overview and comparison of impedance matching networks for inductive WPT system

Impedance matching networks (IMN) are essential in the WPT system for several reasons:

- IMN can be used to compensate for the mismatches due to changes in distance and misalignment.
- IMN can be used to tune a resonant tank for power transfer at an ISM band frequency.
- IMN can be used to compensate for load changes.

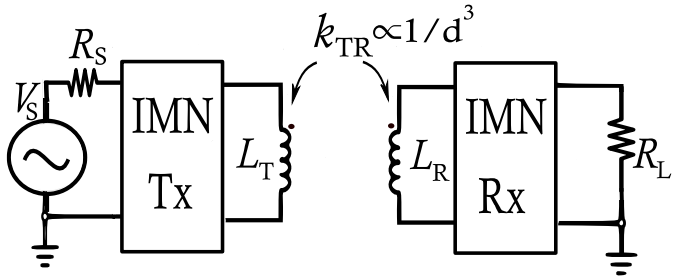

Figure 2.1: An equivalent circuit model of inductive WPT system with Impedance matching networks (IMN).

An equivalent circuit model of the WPT system shown in Fig. 1.5 is shown in Fig. 2.1. An alternating voltage source V_S with internal resistance R_S drives the transmitter coil L_T through the IMN Tx. The coil L_T is magnetically coupled to the receiver coil L_R with coupling coefficient k_{TR}. The coupling coefficient k_{TR} is inverse proportional to the cube of the distance between the coils. Receiver coil L_R is connected to the load resistance R_L through the IMN Rx. The resistance R_L may represent complex circuits such as a rectifier and a battery.

2.1 Conjugate impedance and maximum PTE

A magnetic resonant WPT system can be represented as a two-port network as shown in Fig. 2.2. There are several impedances in this system:

the input impedance Z_{in}, which is the impedance that can be seen from the alternating voltage source V_S, the load impedance Z_L, and output impedance Z_{out}, which is the impedance that can be seen from load side when the input of two-port network is terminated by source resistance R_S. In our study, we assume a symmetrical WPT system, i.e., the load impedance is equal to the load resistance R_L, which is equal to the source resistance R_S.

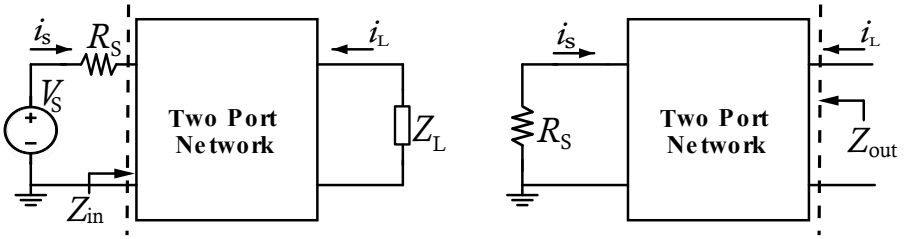

Figure 2.2: A two-port network representation of WPT system: (a) Z_{in} the input impedance when the network is terminated by load impedance Z_L; (b) Z_{out} when the network is terminated by source resistance R_S.

The efficiency of such a system can be expressed as the ratio between the power at the load to the power at the input of the two-port network

$$\eta = \frac{P_L}{P_{in}} = \frac{|S_{21}|^2}{1 - |S_{11}|^2}, \tag{2.1}$$

where $S_{21/11}$ are the scattering parameters [33, 34]. It has been demonstrated that reflection coefficient S_{11} is zero when

$$R_S = Z_{in}^*, \tag{2.2}$$

where Z_{in}^* is a conjugate image of input impedance [35]. If condition (2.2) is satisfied the maximum power transfer efficiency can be achieved

$$\eta = |S_{21}|^2 \tag{2.3}$$

2.2 Frequency splitting

The two-coil inductive WPT system shown in Fig. 2.3 is the simplest way of optimizing the power transfer efficiency. Capacitances C_T, C_R match

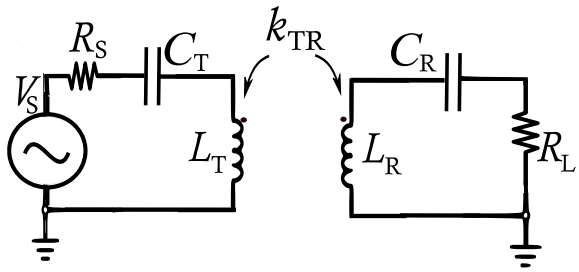

Figure 2.3: An equivalent circuit model of the two-coil WPT system without impedance matching networks (IMN).

the system for a given optimal distance d_0 between resonators at a given resonance frequency f_r.

Distance d_0 is the distance where the coupling between coils is optimal, referred to as critical coupling k_c. If the distance decreases compared to the optimal distance d_0, the coupling coefficient k_{TR} between transmitter coil L_T and receiver coil L_R increases. The region where the coupling coefficient is higher than the critical coupling k_c is referred to as the over-coupled region. This over-coupling results in a phenomenon called frequency splitting, as shown in Fig. 2.4. In this figure, the dependency of $|S_{21}|^2$ values on coupling coefficient k_{TR} and operation frequency are plotted for the two-coil WPT system shown in Fig. 2.3. The parameters used for the simulation of the system are given in Table 2.1. As the distance, d between coils L_T and L_R increases compared to the optimal distance d_0, the coupling coefficient k_{TR} between coils decreases. This is referred to as the under-coupled region.

Table 2.1: Parameters of two-coil WPT system.

Parameter	**Values**	Units
$R_S = R_L$	50	Ω
$C_T = C_R$	6.9	pF
$L_T = L_R$	20	μH
f_r	13.56	MHz

In the over-coupled region where the frequency splitting occurs, the magnetic flux between coils is more than required [20] for optimal operation. In Fig. 2.4, at the critical coupling coefficient $k_c = 0.03$, the frequency separation is merged into one maximum efficiency point at

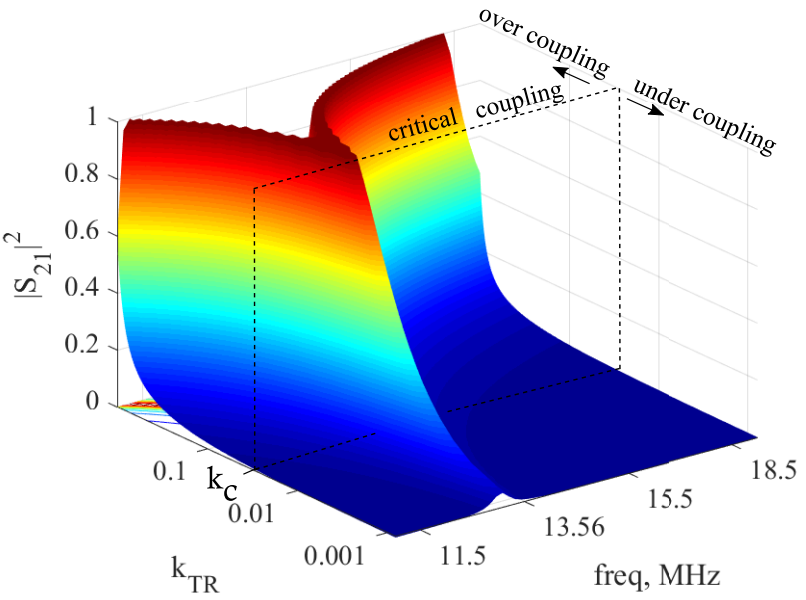

Figure 2.4: $|S_{21}|^2$ versus coupling coefficient k_{tr} and operation frequency.

resonant frequency of 13.56 MHz. At longer distances, i.e., in the under-coupled region, the flux between coils is insufficient to deliver all the power from transmitter coil L_T to the receiver L_R. The increase in the distance also results in an impedance change in the system, which needs to be compensated using a proper IMN. Therefore, power transfer efficiency drops rapidly as distance increases.

As mentioned in the previous chapter, there are mainly two types of IMN techniques that can be used to compensate for distance changes between the coils to maintain the maximum power transfer: inductive IMN and capacitive IMN. The performances of these matching approaches are discussed in detail in the following subsections.

Inductive IMN

The equivalent circuit model of a four-coil magnetic resonant WPT system is shown in Fig. 2.5. The system consists of two high-Q resonating coils L_T and L_R. L_T is coupled to and driven by a low-Q coil L_S connected to the alternating power source V_S, Fig. 2.5. The coil L_R is coupled to the low-Q coil L_L, which is connected to the load R_L. The coupling between resonator coils and the low Q coils k_T and k_R can be

considered as parts of an impedance matching network. Impedance tuning can be achieved by varying k_T and k_R. This system can therefore be considered as a system with inductive matching as in our study.

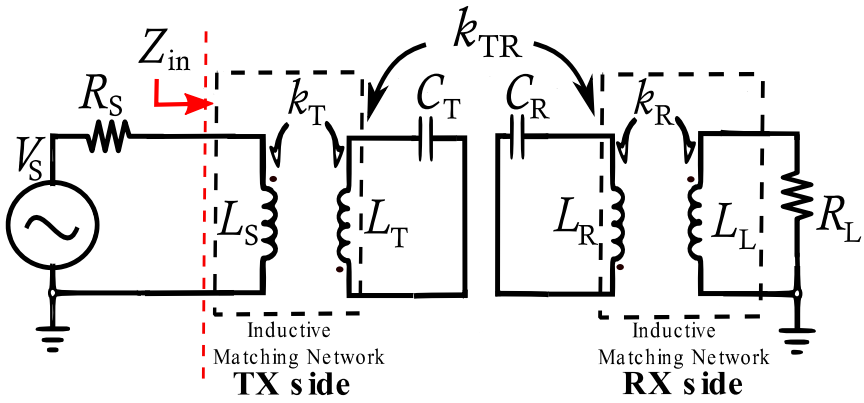

Figure 2.5: Equivalent model of WPT system with inductive IMNs at transmitter and receiver sides.

In this method, couplings between load coil L_L and transmitter coil L_T, as well as between source coil L_S and receiver coil L_R are neglected as these are normally small. The couplings k_T and k_R can be used as parameters in the active IMN. Detailed circuit analysis has been presented in [36], which concludes that power transfer efficiency (PTE) of such system is proportional to the values of couplings k_{TR}, k_T and k_R as

$$\eta \propto \frac{k_T k_R}{k_{TR}} \tag{2.4}$$

It is known that PTE from a source to a system is maximum when the source resistor R_S is equal to the input impedance Z_{in}, which is also valid for the WPT system shown in the figure above. The change in distance and therefore the coupling coefficient k_{TR} changes the value of the impedance Z_{in}, which can be compensated by values of the k_T and/or k_R according to eq. (2.4).

In Fig. 2.6, the relation between $|S_{21}|^2$ and coupling coefficients k_T, k_R, k_{TR} is shown. Simulation is performed by symmetrically varying values of coupling coefficients k_T and k_R at 13.56 MHz. Here, we can see that the critical coupling coefficient k_c is lowered to 0.005 compared to the previous result where $k_c = 0.03$ as in Fig. 2.4 which is due to the added couplings k_T, k_R. However, by adjusting the values of the

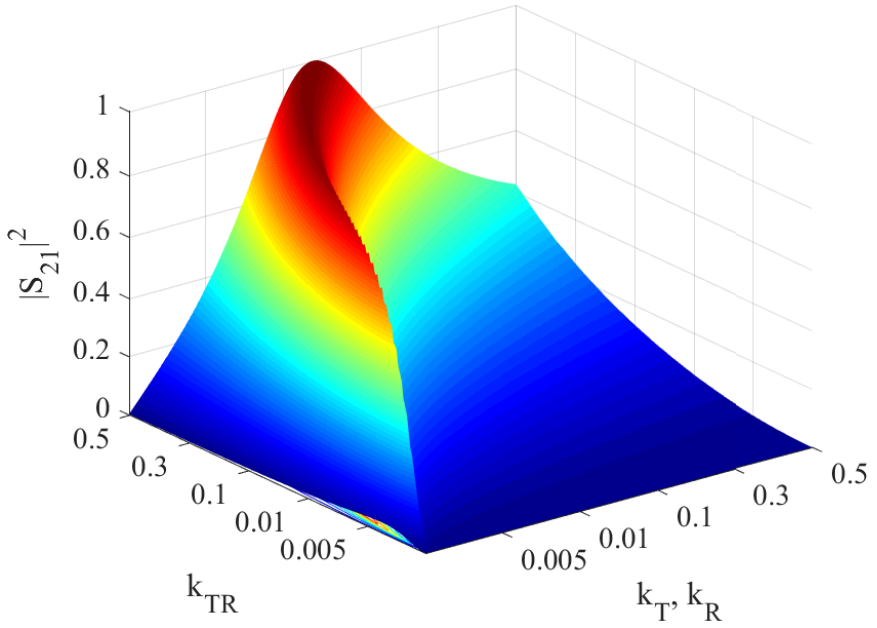

Figure 2.6: $|S_{21}|^2$ versus coupling coefficient k_{tr} and coupling coefficients k_T and k_R.

couplings k_T and k_R for the corresponding coupling coefficient k_{TR}, the frequency splitting in over coupling region can be avoided. When the distance increases, the coupling decreases. The distance change between resonating coils is inverse proportional to the value of coupling coefficient k_{TR}, which implies that in order to increase the distance between transmitter and receiver, it is required to lower the coupling coefficients k_T, k_R. Likewise, for shorter distances, higher coupling coefficients k_T, k_R are required.

Capacitive IMN

The most popular and common IMNs are based on capacitive matching techniques. The equivalent model of the WPT system with an L-type capacitive IMN is given in Fig. 2.7. Impedance changes can be matched by varying values of the in-series capacitors C_{ts}, C_{rs} and the in-parallel capacitors C_{tp}, C_{rp}, both at the transmitter and receiver sides.

The dependence between $|S_{21}|^2$, coupling coefficient k_{TR} and capacitance change at 13.56 MHz is presented in Fig. 2.8. The system is consid-

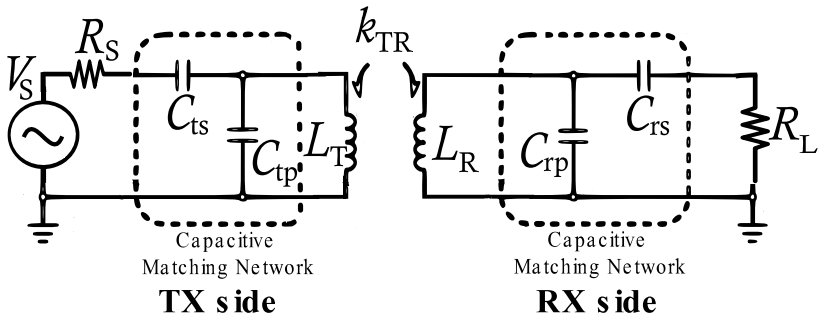

Figure 2.7: Equivalent model of WPT system with capacitive IMNs at transmitter and receiver sides.

ered symmetrical as in the previous examples, and the capacitances are adjusted in the same way in both transmitter and receiver sides with the assumption that $C_{ts} = C_{rs} = C_S$ and $C_{tp} = C_{rp} = C_P$. A capacitance

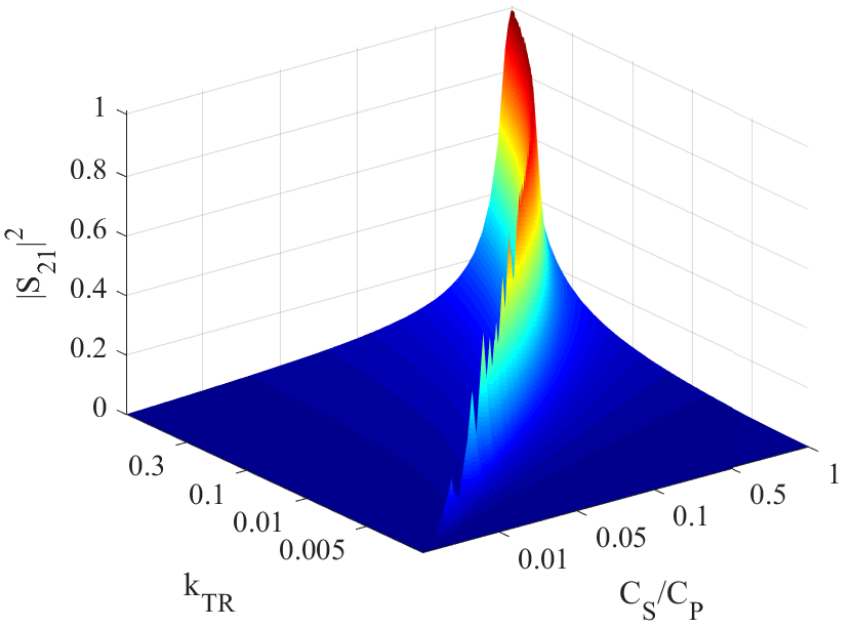

Figure 2.8: $|S_{21}|^2$ versus coupling coefficient k_{tr} and ratio between series and parallel capacitances C_S/C_P.

change is represented by the ratio between series and parallel capacitances C_S/C_P. The capacitive method also shows improvement in the

critical coupling coefficient value of k_c, which is around 0.005. The illustration demonstrates that frequency splitting phenomena can be solved as well. For farther distances, series capacitance C_S value should be decreased in relation to the value of parallel capacitance C_P, whereas for closer distances, the value of C_S should be increased.

2.3 Comparison of capacitive and inductive IMNs

Impedance matching networks for inductive WPT may vary depending on applications. Our first work was focused on the comparison of the most popular matching techniques, i.e., the capacitive and inductive matching networks. This analysis was chosen due to the lack of a good quality review paper on the existing IMNs for wireless power transfer, which compares these methods. Moreover, there is a challenge in the direct comparison of their matching performances because of their fundamentally different circuit topologies. The conference paper, Article I (see Appendix 1), demonstrates that both approaches could potentially achieve a similar matching level in certain cases. In the consequent journal paper, Article III (see Appendix 3), we compare these matching networks over a full range of realistic parameters for three different applications distinguished by their operating frequency and power level: case A, a car charging system, case B a tablet charging system and a high-frequency application as case C. Their applications and parameters are given in the article. The circuits are modeled as in Fig-s. 2.5 and 2.7, which consists of source resistance R_S, matching networks (capacitive or inductive), and lossless coils for transmission and reception.

The article proposes a method that makes a systematic comparison of their performance possible. The proposed method is based on a comparison of the conjugate impedance of the matchable load displayed in the Smith chart. Fig. 2.9 demonstrates the realizable reflection coefficient values in the Smith chart for the car charging system. The matchable regions are indicated by bold black borders. Each figure consists of three impedance regions, where each region corresponds to different resulting impedances in the circuit: Ztx—impedance at the transmitter, Ztr—impedance after transmission, and Zout—impedance at the output. The impedance ranges are obtained by sweeping IMN parameters over the realistic range of values. The IMN parameters are self-inductances of source and load coils L_S, L_L and coupling coefficients k_S, k_T for inductive IMN and series and parallel capacitances $C_{ts/rs}$, $C_{tp/rp}$ for capacitive

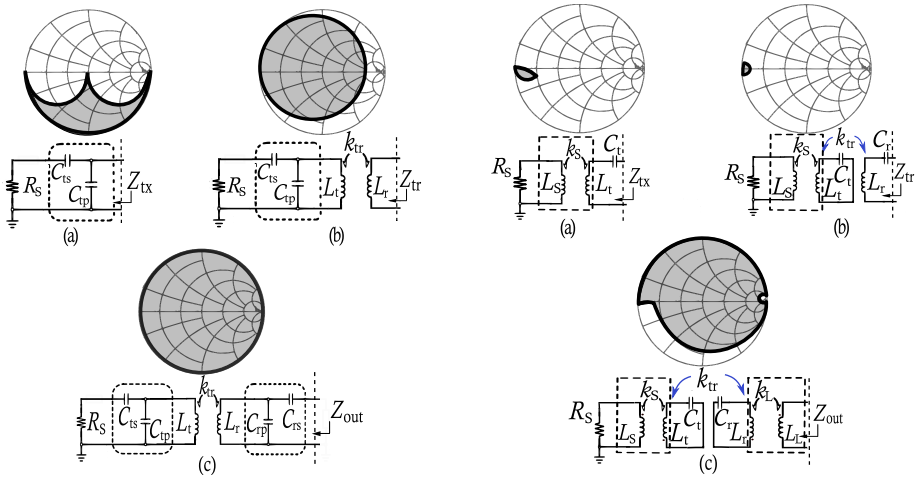

Figure 2.9: Reflection coefficient graphs show impedances that can be obtained by capacitive (left) and inductive (right) matching networks placed into WPT system for car charging system: (a) Ztx—impedance at the transmitter, (b) Ztr—impedance after transmission, (c) Zout—impedance at the output. The result is taken from Article III.

IMN.

According to this research, impedance matching networks provide quite different areas of perfectly matchable impedances, which is highly dependent on operation frequency. Moreover, the comparison showed that both methods offer comparable power transfer when the networks are optimized for loads. The paper's outcome has shown that both matching networks can be equally effective in matching different load values.

3 Proposed inductive IMN for magnetic resonance WPT

As discussed earlier in this thesis and the published papers (see Appendix I, III), the change in the mutual inductance between coils in the inductive IMN can be used as impedance matching. This implies that an active impedance matching can be achieved by making the driving and load coils tunable. Therefore, we propose new discrete inductive IMN designs for the driving and the load coils, where different inductances can be selected using switches. The results of this work have been published in subsequent conference papers (see Appendix II, IV) and journal V. The equivalent circuit model of such a system is shown in Fig. 3.1. The system consists of two high Q-factor resonator coils (L_T, L_R) where the L_T is driven by a set of individually selectable low Q-factor coils denoted L_V. The coils L_V are connected to the power source at the transmitter side. The load is also connected to a set of similar low Q-factor coils and denoted L_V at the receiver side, as shown in the figure. The coupling coefficient k_T between transmitting resonant L_T and the driving coils L_V, and the coefficient k_R between the load coil L_V and the receiver resonant L_R can be considered as transformer-based matching networks [19].

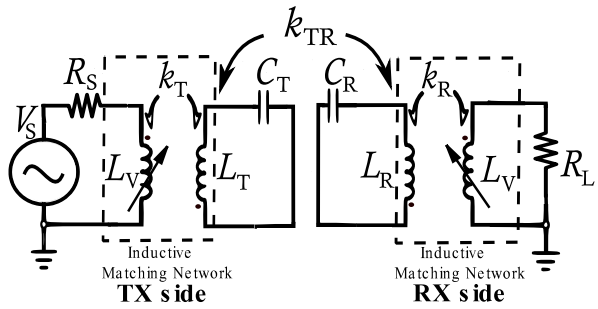

Figure 3.1: Equivalent model of the four-coil magnetic resonance WPT system.

3.1 Multi-loop inductive IMN

In this section, existing adaptive inductive IMN based on selectable coils for improving WPT efficiencies is presented and discussed. This approach is also referred to as a multi-loop inductive IMN for Magnetic Resonant WPT [37–39].

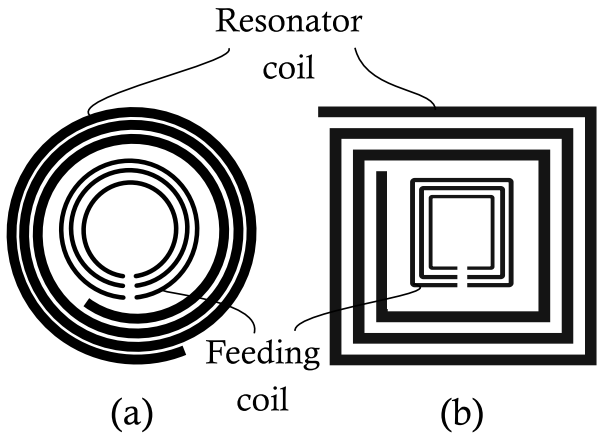

Figure 3.2: Multi-loop inductive IMN: (a) circular multi-loop IMN; (b) rectangular multi-loop feeding.

As shown in Fig. 3.2, the inductive IMN consists of two parts, the resonator coil and the feeding (driving) coils. Similar inductive IMN is used at both the transmitter and receiver side. The feeding coil connects to the voltage source at the transmitter side and to the load at the receiver side. Resonator coils are connected to external capacitors to be tuned at a resonance frequency within the ISM bands. The feeding coil is made of a set of coils with different sizes and self-inductances. By switching between them, the coupling to the resonator coil can be changed. This tuning helps maintain high efficiency throughout the distance changes and misalignment between resonator coils at the receiver and transmitter sides.

Both square and circular methods have been reported in the literature and show an improvement in power transfer efficiency over distance change between transmitter and receiver. These multi-loop systems have their limitations, they are bulky as they require a large size resonator coil, and the self-inductances of driving coils are limited due to the limited inner space of the resonator coil. For instance, in [38] four single square loop coils are placed in the inner region of the high-Q resonator coil with a 68 cm outer diameter. In this scenario, mutual inductances between the resonator and single coils are limited to the range 22nH - 107nH. Moreover, the 68 cm diameter size is quite large to implement in compact electronic devices. It is also true for the system described in [39], where an 8 cm wide square-spiral coil is introduced. The tuning range of 5 inductors placed inside of the square-spiral coil is limited

between 77 and 176 nH. The main drawback of such a system is that the coupling of single loops to the resonator coil decreases dramatically as coils get smaller because the distance between resonator and driving coils increases rapidly.

With these key points in mind, we proposed novel inductive IMNs – switchable multi-coil and interspiraled coil techniques, which offer a larger range of tunability and high coupling for all driving coils. Both methods have a simple design procedure and can be implemented on a two-sided PCB, which makes them compact and potentially low cost.

3.2 Switchable multi-coil and interspiraled coil design

First, we proposed a design of switchable multi-coil inductor and resonant coil as shown in Fig. 3.3. The switchable driving coil consists of ten loops, which are numbered 1 to 10 and located at the front side of the PCB. The radius of the loops is varied from 1 to 10 cm, i.e., 1 cm for the smallest loop and 10 cm for the largest loop. At the backside of the same PCB, a high-quality resonant coil with a spiral shape is placed. The coil sizes and other parameters of the PCB are given in Article II. The coils are implemented on FR4 substrate PCB since it offers an easy fabrication process, low cost, and compactness. However, the structure introduced a parasitic capacitance between the front and back sides of the PCBs, which was eliminated in our consequent solution.

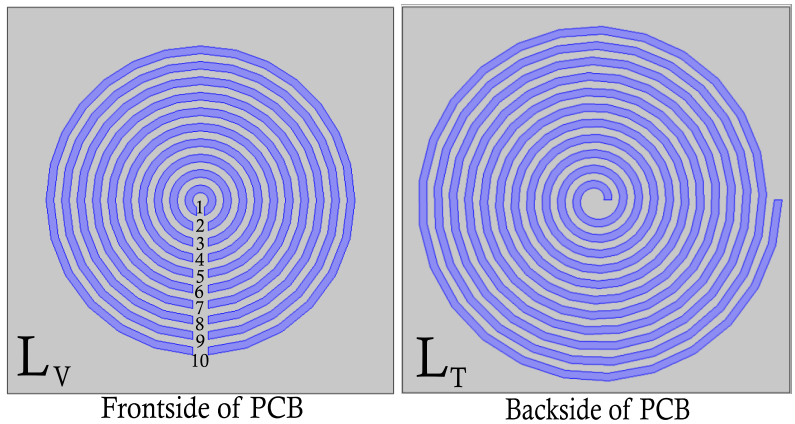

Figure 3.3: Design of the switchable multi-coil (frontside) and resonant coil (backside) on the PCB.

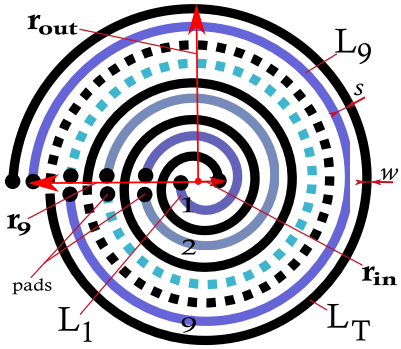

Figure 3.4: The switchable interspiraled coils $L_1 - L_9$, numbered from 1 to 9, and the resonator coil L_R on the same side of PCB. Black dash dots represent turns of resonator coil and colored ones, the interspiraled coils $L_3 - L_8$. Black circles are pads. r_{out} is the outer radius, r_{in} is the inner radius and r_9 is the radius of the ninth driving coil.

The second solution is an interspiraled-coil design, as shown in Fig. 3.4. The system is made of several single loop coils placed in between the turns of the spiral-shaped resonator coil. Nine single turn coils with increasing radius, each numbered from 1 to 9, as shown in the figure. Parameters of interspiraled and spiral-shaped coils are listed in Article II. By choosing the different single-loop coils, the interspiraled coils can be used as an inductive IMN circuit for magnetic resonance WPT both at the receiver and the transmitter side. As all the coils are placed on one side of a PCB, the other side of the PCB can be used for other necessary electronic circuitry such as the amplifier, control system, and their connections which makes the system compact. This interspiraled coil suffers less from parasitic capacitance as no coils cross each other, and therefore, coupling between interspiraled coils is minimized.

Both solutions can be modeled in the same way as a four-coil magnetic resonance WPT system but with multiple driving and load coils. Selecting the different single coils results in different mutual inductances, which can be used to compensate for distance changes and misalignment between resonators. Each driving coil can be selected using switches controlled by a control system.

To simplify the explanation of the working principle of the switchable system, a three-loop model of it is shown in Fig. 3.5. The circuit realization on PCB is given in Fig. 3.5(a), and an equivalent circuit model of inductive IMN is presented in Fig. 3.5(b). Here, L_1 is self-inductance

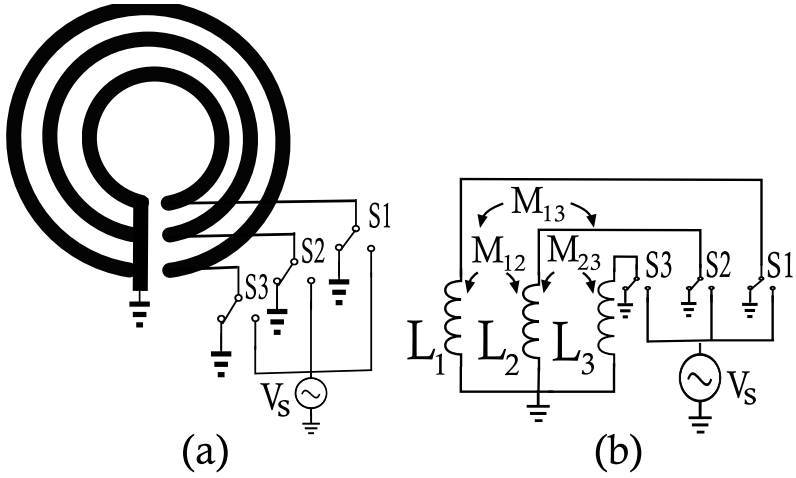

Figure 3.5: Working principle of the switchable coil with three loops: (a) is the realization of the circuit and (b) is the circuit model of it.

for the outer loop, L_2 for middle loop, and L_3 for inner loop. Switches can connect each coil to the power source V_S or ground them for deactivation. The desired inductance of the driving coil can be selected via a set of switches.

3.3 Circuit analysis for multi-coil WPT system

The switchable coils presented in this work can tune the system from one side, i.e., either the receiver or transmitter side or from two simultaneous sides at both the transmitter and the receiver side. For analyzing each case, two different WPT systems are chosen, and an expression for the power transfer efficiency for each case is derived. First, we start the analysis with a three coil system that can be tuned only from the transmitter side. In this system, the source is connected to a switchable coil which drives the resonating transmitter coil, while the resonance coil at the receiver side is connected directly to the load.

The modeling of a four coil system is used for analyzing the two side tuning, i.e., when both transmitter and receiver are connected to a switchable coil. All of these analyses are presented in the following sections.

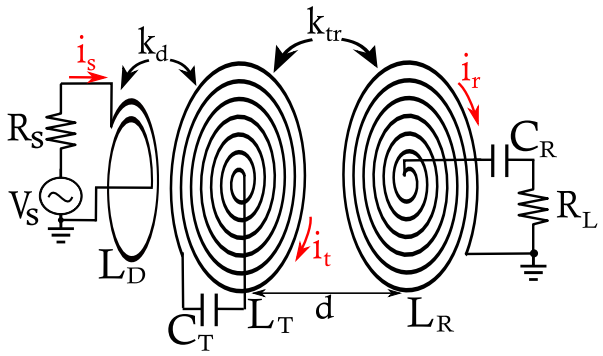

Figure 3.6: The three-coil WPT system: L_D - driving coil, L_T - transmitter coil, L_R - receiver coil, d - distance between coils.

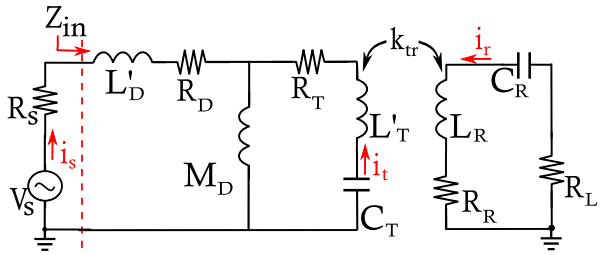

Figure 3.7: The circuit representation of the three-coil WPT system: L_D - driving coil, L_T - transmitter coil, L_R - receiver coil, $C_{T/R}$ - external capacitor.

Three-coil WPT system for tuning at transmitter side

The three-coil WPT system's schematic view is shown in Fig. 3.6. Alternating voltage source V_S with input resistance R_S is driving the interspiraled coil L_D. The driving coil L_D is magnetically coupled with the coupling coefficient k_d to the transmitter coil L_T. The transmitter coil L_T and the receiver coil L_R are placed at a given distance d, which defines the coupling coefficient k_{tr} between them. Coils have parasitic resistances R_D, R_T and R_R. Transmitter and Receiver coils have series connections to external capacitors C_T and C_R respectively, for tuning to resonance. C_T, C_R are chosen to establish a resonance effect at 6.78 MHz, which is within the allowed ISM band. The load resistance R_L and receiver resonator are connected in series.

Circuit view of Fig. 3.6 is given in Fig. 3.7, where $M_D = k_d\sqrt{L_T L_D}$ is the mutual inductance between the driving coil L_D and the transmitter

coil L_T. A T equivalent model of a transformer is used for modeling the coupling between L_D and L_T [40]. Currents and voltages of the circuit can be written using the KVL as

$$V_S = R_S i_s + Z'_D i_s + j\omega M_d(i_s + i_t), \tag{3.1}$$

$$0 = Z'_T i_t + j\omega M_d(i_t + i_s) + \frac{1}{j\omega C_T} i_t - j\omega M_{tr} i_r, \tag{3.2}$$

$$0 = (R_L + Z_R + \frac{1}{j\omega C_R}) i_r - j\omega M_{tr} i_t, \tag{3.3}$$

where $Z'_{D/T}$ is

$$Z'_{D/T} = j\omega L'_{D/T} + R_{D/T} = j\omega(L_{D/T} - M_D) + R_{D/T}, \tag{3.4}$$

and Z_R is receiver coil impedance

$$Z_R = R_R + j\omega L_R, \tag{3.5}$$

mutual inductance between transmitter and receiver coils

$$M_{tr} = k_{tr}\sqrt{L_T L_R}. \tag{3.6}$$

The coupling coefficient k_{tr} is inverse proportional to the cube of distance d between transmitter and receiver coils [41]. Power transfer efficiency of the system can be defined as the ratio between power delivered to the load and input power

$$\eta = \frac{P_L}{P_{in}} = \frac{R_L * |i_r|^2}{R_{in} * |i_s|^2}, \tag{3.7}$$

where R_{in} is real part of Z_{in}, which is an input impedance shown in Fig. 3.7 [33]. Replacing current values from (3.1)-(3.3) to (3.8) and using the equation for the resonance effect

$$\omega L_{T/R} = \frac{1}{\omega C_{T/R}}, \tag{3.8}$$

PTE η can be rewritten as

$$\eta = \frac{R_L \omega^4 M_D^2 M_{TR}^2}{R_{in}(R_R + R_L)^2(R_T + Z_{ref})^2}, \tag{3.9}$$

where Z_{in} is input impedance

$$Z_{in} = Z_D + \frac{\omega^2 M_D^2}{R_T + Z_{ref}}, \tag{3.10}$$

and $Z_D = R_D + j\omega L_D$. Here, Z_{ref} is reflected impedance from receiver side

$$Z_{ref} = \frac{\omega^2 M_{tr}^2}{R_L + R_R}. \tag{3.11}$$

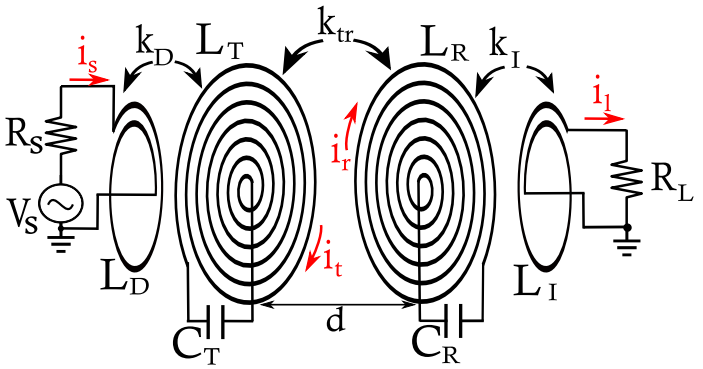

Figure 3.8: The four-coil WPT system: L_D - driving coil, L_T - transmitter coil, L_R - receiver coil, L_L - load coil, d - distance between coils.

Four-coil WPT system for two sided tuning

The four-coil WPT system is shown in Fig. 3.8. Alternating voltage source V_S with input resistance R_S is driving the interspiraled coil L_D. The driving coil L_D is magnetically coupled to the transmitter coil L_T with a coupling coefficient k_D. The transmitter coil L_T and receiver coil L_R are placed at a distance d apart, which relates to the coupling coefficient k_{tr} between them. Load R_L is connected to the interspiraled coil L_I, which is magnetically coupled to the receiver coil L_R with coupling coefficient k_I. Coils have parasitic resistances R_D, R_T, R_R and R_I. Transmitter and Receiver coils have series connections to external capacitors C_T and C_R, respectively. Values of capacitors C_T, C_R are chosen to establish a resonance effect at 6.78 MHz, which is within the allowed ISM bands, and standard operating frequency suggested by AirFuel Alliance [42]. Load resistance R_L and receiver coil L_R are connected in series.

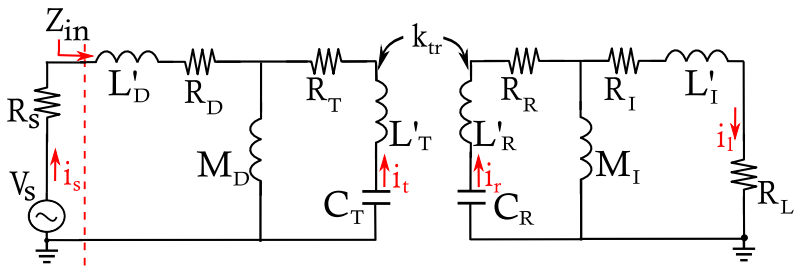

Figure 3.9: The circuit representation of the four-coil WPT system: L_D - driving interspiraled coil, L_T - transmitter coil, L_R - receiver coil, L_I - load interspiraled coil, $C_{T/R}$ - external capacitor.

Similarly to the case with the three-coil system, a circuit representation of four-coil is required for the circuit analysis, which is given in Fig. 3.9. Equation (3.9) can be modified for the four coil system using the reflected impedances

$$\eta = \frac{R_L Z_{refT} Z_{refR}}{R_{in}(R_R + R_L)(R_T + Z_{refR})}, \tag{3.12}$$

where Z_{refT} and Z_{refR} are reflected impedances from transmitter and receiver coils, respectively, and equal to

$$Z_{refR} = \frac{\omega^2 M_{tr}^2}{R_L + R_R}, \tag{3.13}$$

$$Z_{refT} = \frac{\omega^2 M_D^2}{Z_{refR} + R_T}. \tag{3.14}$$

So, for four-coil WPT system in Fig. 3.9 a PTE expression is

$$\eta = \frac{R_L |Z_{refT} Z_{refR} Z_{refI}|}{R_{in} |(R_T + Z_{refR})(R_R + Z_{refI})(Z_I + R_L)|}. \tag{3.15}$$

Here, Z_{refI}, Z_{refR},Z_{refT} and Z_{in} are reflected impedances from the magnetic couplings

$$Z_{refI} = \frac{\omega^2 M_I^2}{R_L + Z_I}, \tag{3.16}$$

$$Z_{refR} = \frac{\omega^2 M_{tr}^2}{Z_{refI} + R_R}, \tag{3.17}$$

$$Z_{refT} = \frac{\omega^2 M_D^2}{Z_{refR} + R_T}, \tag{3.18}$$

$$Z_{in} = Z_D + Z_{refT}, \tag{3.19}$$

where $Z_I = j\omega L_I + R_I$ is the impedance of interspiraled coil connected to the load.

3.4 Mutual inductance and self-inductance analysis

According to PTE expressions in (3.9) and (3.15), the efficiency is directly dependent on self-inductance and mutual inductance of the inductive IMN. Therefore, this section presents simulation and measurements on the inductances of multi-coil and interspiraled-coil inductive IMN shown in Figs. 3.3 and 3.4.

The self-inductances of the ten-loop switchable multi-coil IMN (Fig. 3.3) are analyzed in Article II. The switchable multi-coil system is simulated at 6.78 MHz using COMSOL Multiphysics. Linear growth of the inductance can be seen between loops 4 and 10. There is a non-linearity between loops 3 and 1, which we believe is due to their position related to the resonating coil. Nevertheless, the relative variation of the inductance from 19 nH to 373 nH is achieved, which gives a better tunability range compared to the existing multi-loop models discussed above. The self-inductance of the spiral coil is $L_T = 9.6$ μH.

In Article II, we gave a comparison of simulated and measured values of mutual inductance between the transmitter coil L_T and the corresponding loop L_V, which is shown in Fig. 3.10. Measurement has been obtained by using high precision GW-Intek LCR meter. Simulated values are represented by stars which are connected by a solid curve, whereas measured values are shown by plus signs and a dashed curve. According to the measured results, mutual inductances are varied from 25 nH to 1230 nH. Moreover, an almost linear behavior of the trace can be seen for both parameters, with a small deviation between simulation and measurement results. The deviation can be explained by parasitic components introduced in the measurement setup and/or inaccuracy during the fabrication process.

Research on the mutual inductances between the interspiraled coils and the resonator coil was the focus of Article IV. The structure given in Fig. 3.4 is simulated in COMSOL Multiphysics. A comparison between the measurement and the simulation results at frequency = 100 kHz is shown in Fig. 3.11. 100KHz was chosen due to frequency limitations in our measurement tool. The linear increase of the measured mutual inductance can be noticed between M_1 and M_8, which is comparable with

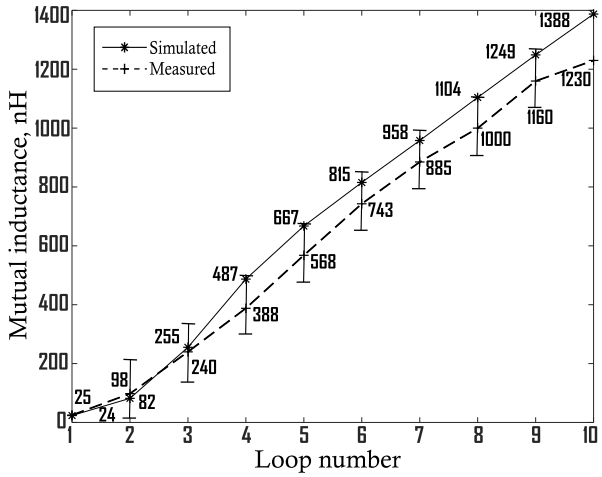

Figure 3.10: Simulated and measured mutual inductance between the switchable driving L_V and resonant L_T coil at 2 kHz. The result is taken from Article II.

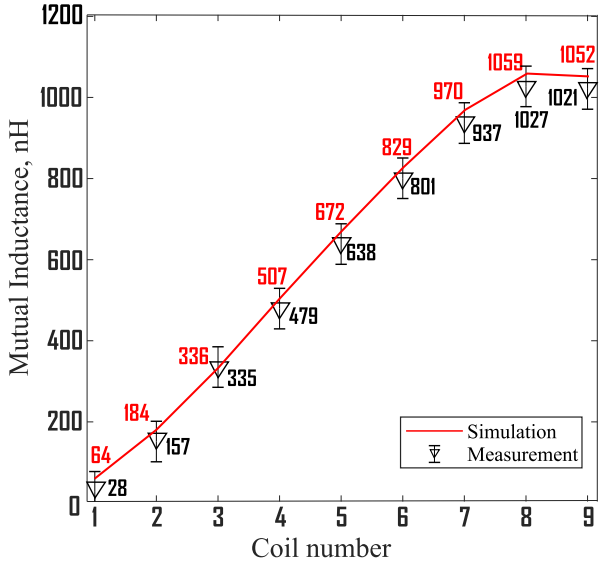

Figure 3.11: Simulated and measured mutual inductances $M_1 - M_9$ between the driving coils $L_1 - L_9$ and the resonator coil L_R at 100 kHz. The result is taken from Article IV.

the simulation results highlighted in red. Both for the measurement and the simulation, the linearity breaks up at coil 9, i.e., the largest coil. Moreover, in the following section, where the efficiency performance of

the inductive IMN is analyzed, it is shown that coil nine is not improving the power transfer efficiency further. Mutual and self-inductances of interspiraled-coils used as transmitter-side inductive IMN are also simulated at the operation frequency of 6.78 MHz, and the results are presented in Article V.

The multi-coil and the interspiraled coils can be designed to achieve the desired range of the mutual inductance at different operating frequencies. The linearity of the mutual inductance can be improved by a more careful design of the coil parameters. The tuning range can be increased by driving several coils simultaneously, either in series or parallel.

According to the eqs. (3.9) and (3.15), efficiency is also dependent on mutual inductance M_{tr} between the spiral coils. The mutual inductance is dependent on distance and coil size, as shown in Fig. 3.12. Mutual inductance is calculated by numerical method via formula given in [43], which is verified by simulation result from Comsol Multiphysics. The mutual inductance value decreases from 3.4 uH to 0.008 uH when the distance between the coil increases from 2 to 25 cm. However, mutual inductance can be improved by increasing the radius/turns of the spiral coil. Growth in the diameter of the coil affects the compactness of the system, which means a trade-off between the size of the coil and operating distance.

3.5 Simulation of PTE

This section presents an estimation of power transfer efficiency (PTE) η from the circuit analysis and simulation in Comsol Multiphysics. Efficiency is plotted versus distance between resonator coils, with a distance variation between 2-25 cm. The efficiency drops below 1% after 25 cm of distance, making it negligible. The calculations are performed for cases when driving the interspiraled coils 2 to 9. The driving of interspiraled coil 1 is excluded from the results since the efficiency of the system is below 5%. In this section, a symmetrical WPT system with $R_S = R_L = 50\ \Omega$ is considered. Load variation is spotlighted in Article V.

Fig. 3.13 shows calculated PTE η versus distance using equation (3.9) for the three-coil WPT system. The graph demonstrates that the optimal matching distance is between 8-10 cm, and larger driving coils perform better than smaller ones. Efficiency drops from 93% offered by coil 8 to 4% offered by coil 2 for the same optimal distance. Despite the

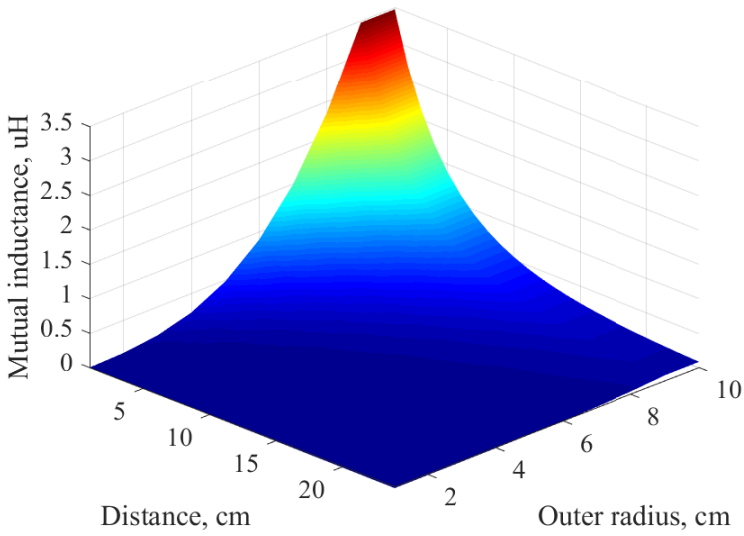

Figure 3.12: Mutual inductance M_{tr} vs distance vs outer radius of the spiral coil.

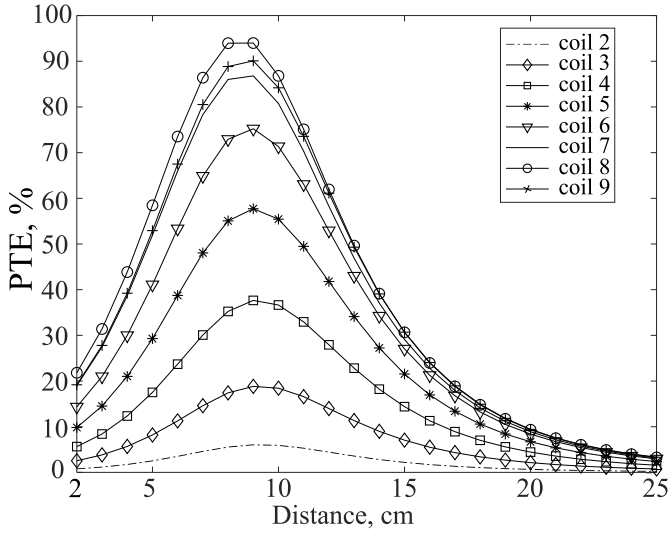

Figure 3.13: Simulation of the derived formulas of relative efficiency versus distance at 6.78 MHz for the three-coil WPT system. The figure shows that one side matching is not effective.

larger size of coil nine compared to coil eight, it offers less PTE at the

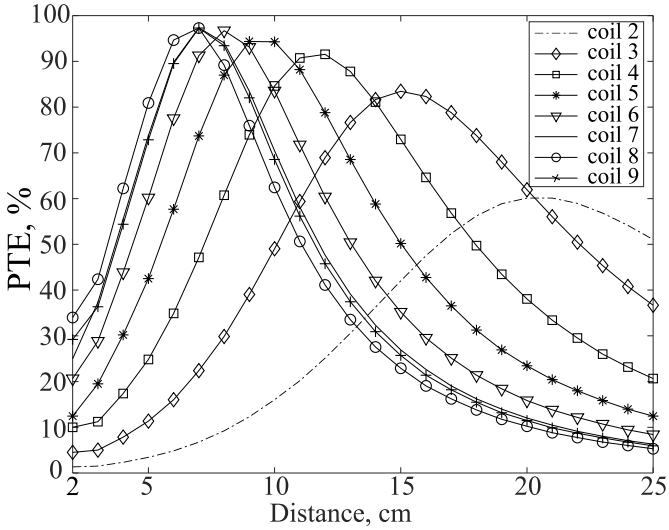

Figure 3.14: Simulation of the derived formulas of relative efficiency versus distance at 6.78 MHz for the four-coil WPT system. The figure shows that two-side matching is very effective.

optimal distance. It is due to the smaller part of the outer magnetic field that covers the resonating coil. This is also evident from Fig. 3.11.

Fig. 3.14 shows the calculated PTE η versus the distance using equation (3.15) for the four-coil WPT system. The graphs display the cases when the driving coil n is used to drive the system at the transmitter side, and the coil n is connected to the load at the receiver side in the same manner, where n is the number of the interspiraled coil between 2 and 9. Compared to the three-coil WPT system, an improvement of PTE in the under-coupled region is noticeable. Switching to the interspiraled coil 2 at 25cm can improve the PTE to more than 50 %, whereas in three-coil WPT, PTE drops to almost 0 %. The optimal distance for the four coil system has been changed to a shorter distance because of the change in impedance in the circuit compared to the 3 coil system.

COMSOL Multiphysics simulation performed on the three coil system is shown in Fig. 3.15, where the distance between two identical PCBs with interspiraled coils is varied from 2 to 25 cm. Each PCB contains a spiral-shaped resonator coil $L_{T/R}$ and interspiraled coils. Driving-coil L_D is connected to port 1, whereas port 2 is directly connected to the receiver resonator coil L_R on PCB 2 (no tuning at the receiver side). The simulated S-parameter values between ports 1 and 2 are used to calculate

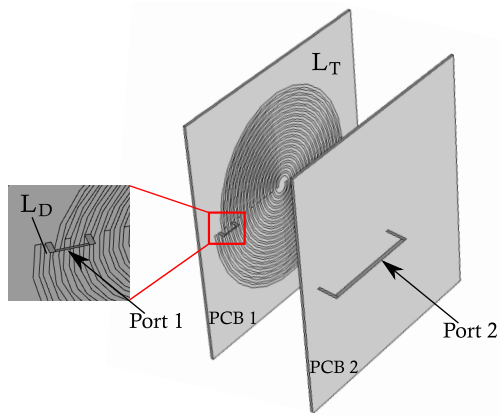

Figure 3.15: Comsol design of interspiraled coils used in the simulation of PTE presented in Articles IV and V.

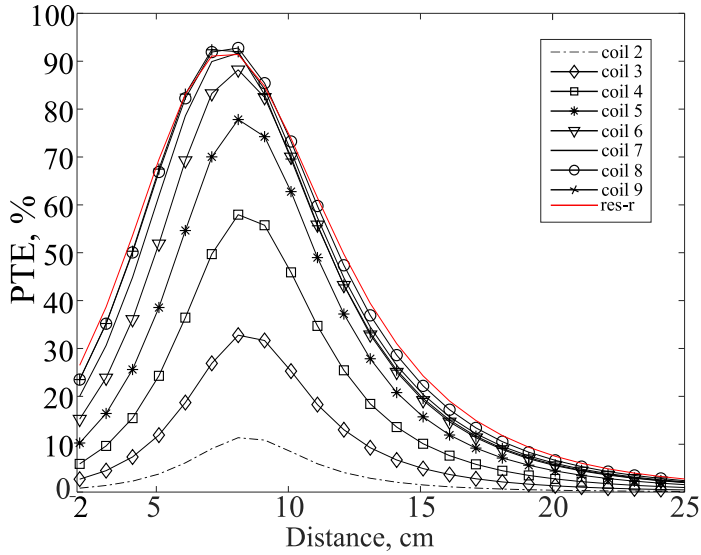

Figure 3.16: Comsol simulation of PTE versus distance at 6.78 MHz. The figure shows that one side matching is not effective. The red curve shows when the source is directly connected to the resonator coil. The result is taken from Article V.

the PTE using eq. (2.4).

PTE versus distance at 6.78 MHz for cases when a single-coil n is active is compared in Fig. 3.16. The red trace on this graph represents a two-coil WPT system, where port 1 is directly connected to the resonator

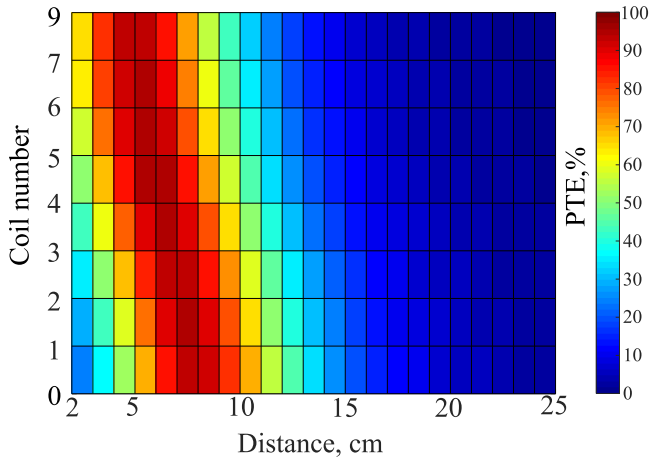

Figure 3.17: Comsol simulation of PTE versus coil 8 and coil n in series at 6.78 MHz. The figure shows that one side matching can be achieved for the over-coupled region when driving two coils in series. The result is taken from Article V.

(transmitter) coil L_T and port 2 to the receiver resonator coil L_R. The highest efficiency is achieved at a distance between 8-9 cm, which is also obtained by circuit analysis shown in Fig. 3.13. The result illustrates that single-coil switching at Tx-side has the same performance as a two-coil WPT system. At distances smaller than 8 cm, the PTE starts to drop, from 92% at 8 cm to 40% at 2 cm distance since it is in the over-coupled region. At 15 cm, it drops down to 50% as it is in the under-coupled region.

In Fig. 3.17, the PTE as a function of the series combination of coil 8 and another coil is demonstrated. Y-axis shows the coil number, which is connected to coil 8 in series. 0 means coil 8 alone, 9 means coil 8 and coil 9 in-series and etc. Color-bar displays the PTE value from 0 to 100 %. The figure shows that there is a PTE improvement of ca. 20-200 % by the series connection of the coils, especially for the over-coupled region. The best result is provided by a combination of coil 9 and coil 8 as it provides 60 % at 2 cm compared to 26 % by driving single coil 8 and 28 % by the two-coil WPT system. Moreover, almost 94 % PTE can be obtained between 3 - 8 cm compared to when only coil 8 is used as in a simple two-coil WPT system. This proves that switching between coils improves the performance of the WPT system when the distance between coils varies in the over-coupled region.

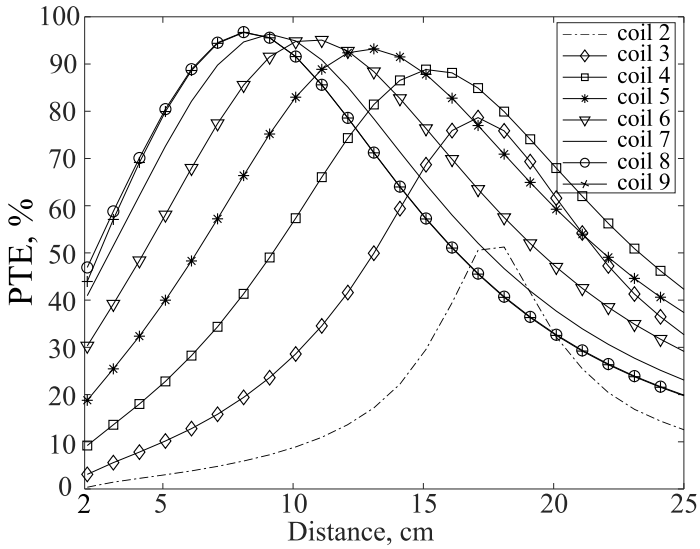

Figure 3.18: Comsol simulation of the power transfer efficiency versus distance at 6.78 MHz for the four-coil WPT system. The figure shows that two-side matching is very effective for matching under- and over-coupled regions.

COMSOL Multiphysics simulation results for a four-coil WPT system are presented in Fig. 3.18. For these scenarios, the driving coils from 1 to 9 are used to feed the four-coil WPT system separately. The optimal distance is varied as in previous cases, from 2 to 25 cm. The load is connected to the symmetrical interspiraled coil at the receiver side. In the over-coupled region, i.e., shorter than the optimal distance, they provide better performance than the two-coil WPT system, shown with a red trace in Fig. 3.16. Moreover, in the under-coupled region, it offers an extensive improvement, which provides a PTE above approximately 50 % efficiency until 23 cm compared to 5 % of the two-coil WPT system. The simulation shows that switching between the interspiraled coils can maintain active matching between 3 to 21 cm with at least 70% PTE.

We have also investigated an impedance mismatch of the WPT system with interspiraled coils at the Tx side. The input impedance versus operation frequency is shown in Fig. 3.19. According to the conjugate matching method, the highest efficiency can be achieved when input impedance is the conjugate impedance of source impedance [33, 34], see the condition (2.2). In a single-sided interspiraled WPT system, the source impedance is R_S, which means the imaginary impedance of the

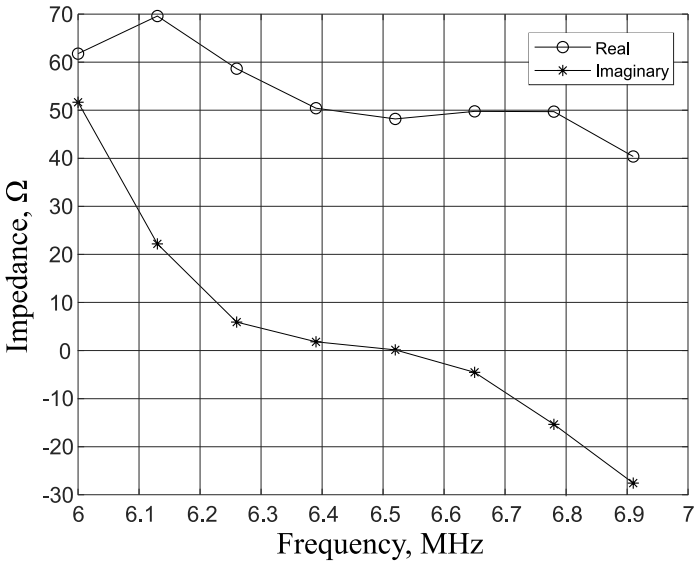

Figure 3.19: Comsol simulation of the input impedance of single-sided interspiraled WPT system.

Z^*_{IN} should be 0. As it can be seen from the graph, the real part of input impedance is 50 Ω, and the imaginary part is -15 Ω. In conclusion, the system is slightly in mismatch, which means efficiency can be further improved by changing the operating frequency to 6.5 MHz or by adding external capacitance to the matching system. The system already offers sufficient efficiency, therefore, we have not implemented either solution. However, we will keep in mind this aspect in our future redesign of the system.

3.6 Measurement of relative efficiency

This section briefly describes the measurement process of relative efficiency and results obtained for Article V. Relative efficiency is defined as the ratio of powers

$$\eta_{rel} = \frac{P_{out}}{P_{ref}}, \tag{3.20}$$

where P_{ref} is the measured power at the load when 50 Ω load is directly connected to the signal generator, and P_{out} is measured power at the same load when WPT system coils are introduced i.e. load is connected

to the receiver side the WPT system. Relative PTE is used to take into account the effect of the wiring in the measurement. PTE described in the circuit analysis, and the simulation sections are clearly different from the relative efficiency η_{rel} used in the measurements, however, as we see from the results given below, they have similar behavior and, therefore, can be used for justification of analytical results. The other measurement option, which would have given us a more accurate value of the PTE, is a setup using the Vector Network Analyser (VNA). Unfortunately, due to the unavailability of the equipment at the time of the measurement, relative PTE was used. However, the VNA method is used once for identifying S-parameters for Article IV, and its result will be discussed later in this section.

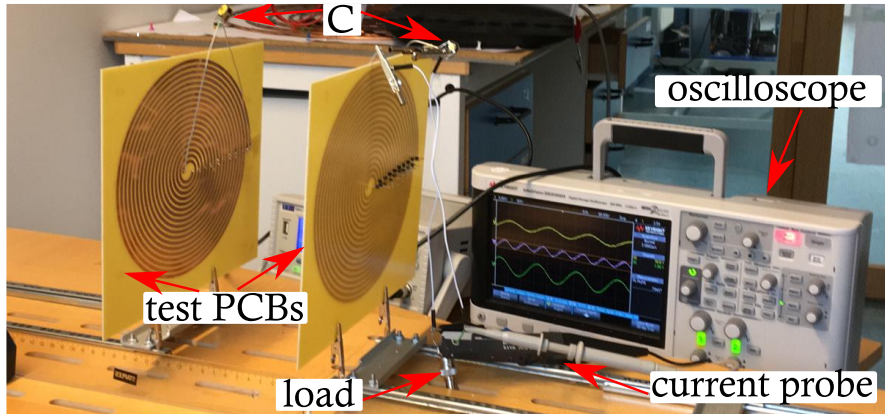

Figure 3.20: Measurement setup for the wireless power transfer system consisting of two interspiraled coils on test PCBs, capacitors placed on a rail for distance variation and oscilloscope, a 50 Ω load, and a current probe. The picture is taken from Article V.

The experimental setup, shown in Fig. 3.20 is used to measure the relative efficiency η_{rel} versus distance, which is varied from 2 cm to 25 cm for each scenario. The setup consists of a two-port oscilloscope, ceramic capacitors, a current probe, and two identical PCBs with coils. The PCBs are mounted on movable rails, where the distance between PCBs can be manually adjusted. Varactors with the capacitance of approximately $C = 68$ pF are connected in series to the spiral coils, so the ISM-band resonance frequency of 6.78 MHz is achieved.

Fig. 3.21 presents the measured relative efficiency η_{rel} from 2 cm to 25 cm distance between resonators. Graphs display efficiencies for the

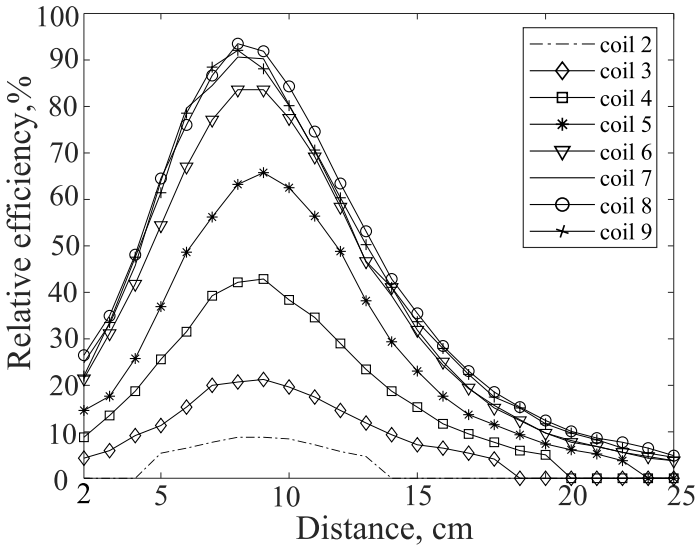

Figure 3.21: Measurement of η_{rel} versus distance at 6.78 MHz when coil n is active. The result is taken from Article V.

three-coil WPT system when the driving coil n (n is the coil number between 2 and 9) is used to drive the system at the transmitter side, and the load is connected to the receiver resonator. Coil 1 is excluded from the graphs as its η_{rel} is very low. The efficiency has a similar trend to the simulation and calculation results given in Figs. 3.13 and 3.16: larger size coils provide the higher η_{rel} at optimal distance, which varies between 8-9 cm.

Results in Fig. 3.21 prove that tuning only the interspiraled coil on the transmitter side is not enough for matching at under-coupled and over-coupled regions. Therefore, we decided to drive several coils simultaneously. Fig. 3.22 demonstrates measurement of η_{rel} for two coils in-series, here coil 8 and coil n, and when load directly connected to the receiver resonator. Immediately, we can notice that the efficiency values are improved by using a combination of coils. Especially at a closer distance than 8 cm, i.e., at the under-coupled region, there is a 40 percent improvement at 2 cm distance. Moreover, results verify our simulation results from Comsol Multiphysics shown in Fig. 3.17. Other series and parallel combinations of interspiraled coils can improve the efficiency further, which has been documented in Article V.

Due to the time constraints of the PhD program, we did not complete the measurements on the usage of interspiraled coils in a four-coil WPT

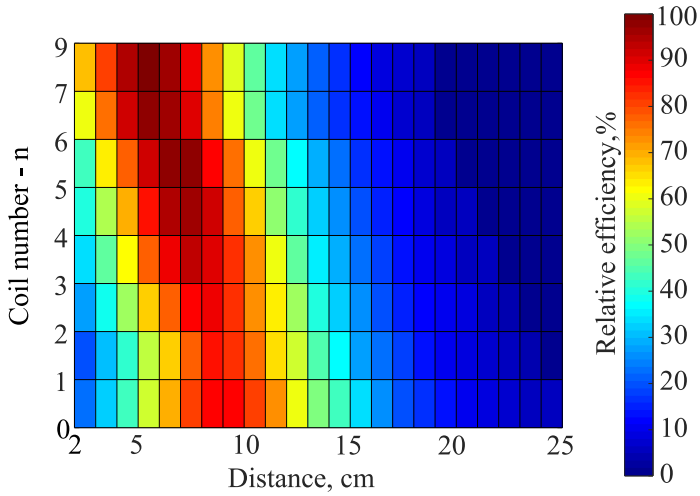

Figure 3.22: Measurement of η_{rel} versus distance at 6.78 MHz when coil 8 and coil n are connected in series. The figure shows that two coils connected in series improve the PTE in the over-coupled region. The result is taken from Article V.

system. Nevertheless, simple measurement results from Article IV reveal several interesting observations for the four-coil WPT system, i.e., two-side matching. This measurement has been completed using a Vector Network Analyzer. Port 1 is connected to the interspiraled coil n on the transmitter PCB and Port 2 to the interspiraled coil n on the receiver PCB. The PTE is estimated via eq (2.4) and presented in Fig. 3.23. The red trace represents a PTE for a typical two-coil WPT system, which means the system without any impedance matching circuitry, thus, only one optimal distance, i.e., approximately 8 cm. We used this red trace as the reference for further comparison of results. At an over-coupled region, closer distances than 8 cm, the PTE starts to drop from 95% to 40% at 2 cm because the coupling coefficient is higher than the optimal one. At 15 cm it drops until 50% as it is in the under-coupled region.

By simultaneously changing the interspiraled coils 1 to 9 on each side, the optimal distance is varied for each case, as shown in Fig. 3.23. In the over-coupled region, the PTE is the same as the reference two-coil WPT system, however, in the under-coupled region, the four-coil WPT system offers an improvement, of PTE, above approximately 50 % efficiency until 22 cm. The measurements show that switching between interspiraled coils can provide active matching between 7 to 17 cm with

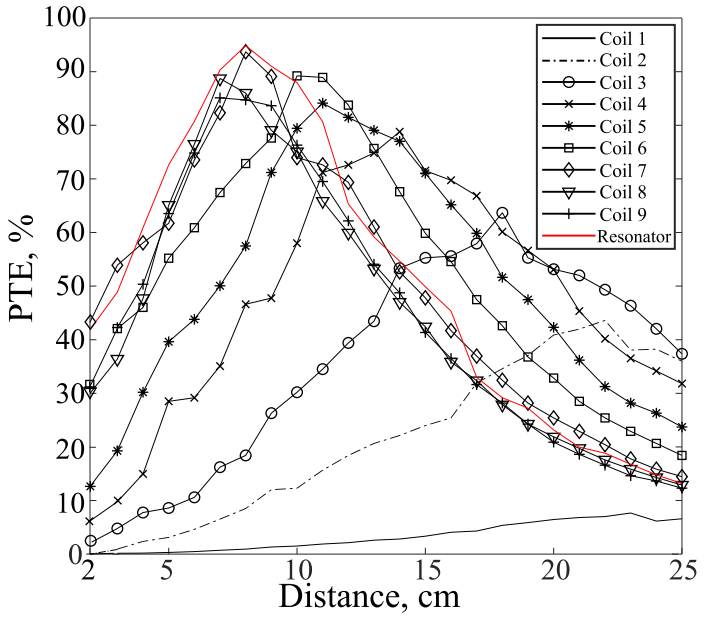

Figure 3.23: Measurement of the PTE versus distance at 5.3 MHz. The result is taken from Article IV.

at least 70% PTE. It also verifies our calculation and simulation results given in Fig. 3.14 and Fig. 3.18, respectively.

3.7 Quality factor of coils

The quality factor (Q-factor) of the coil is a crucial characteristic parameter, which affects the PTE in inductive WPT. In this section, the Q-factor of interspiraled and resonator coils has been presented. Q-factor is calculated via

$$Q = \frac{\omega L}{R}. \tag{3.21}$$

Spiral coils with an increasing number of turns with a constant inner and outer diameter, as shown in Fig. 3.24a were used for calculating the ideal Q factor. The resistance and inductance of each coil are shown in Fig. 3.24b. The relation between the number of turns and Q-factor of the spiral coil without interspiraled coils is shown in Fig. 3.25. It is an almost linear relation, where Q-factor can be increased by adding turns. However, there is a limitation given by the spacing between the turns, which will add parasitic capacitive coupling, and higher resistance due

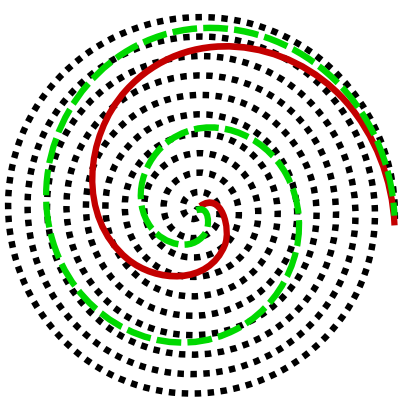

(a) Spiral coils with increasing nr of turns used for calculation.

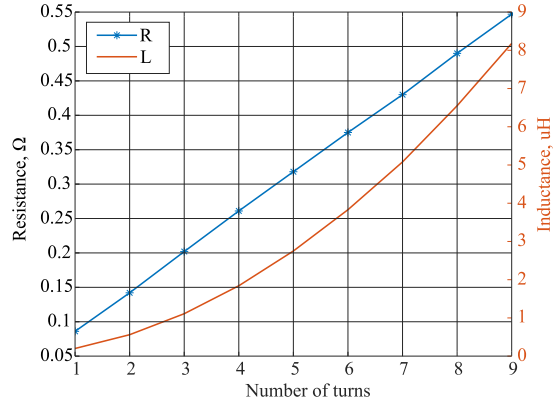

(b) The resistance and inductances for coils in figure (a)

Figure 3.24: Coils for calculating the ideal Q-factor

to increased wire length.

By utilizing data in article V, we can identify values of Q-factor of the coils at 6.78 MHz as shown in Table 3.1. There is a degradation of the Q-factor compared to the simulation result, which is due to the reduction of copper thickness during the fabrication process and parasitics by measurement setup. There is also a noticeable impact on the Q-factor of the spiral coil from the couplings with interspiraled coils as it decreases the Q-factor from ca. 630 to 351.

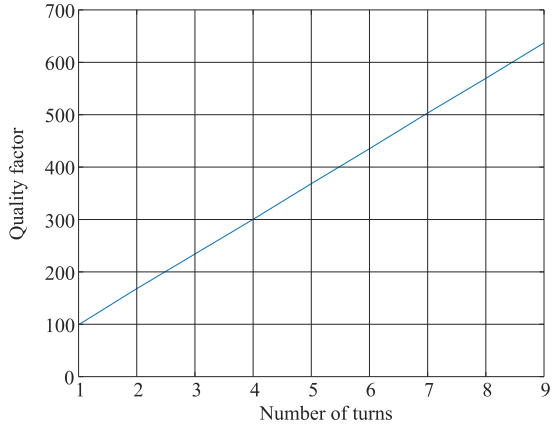

Figure 3.25: Quality factor versus number of turns for spiral coil $L_{T/R}$ without inner coils.

Table 3.1: Driving and resonator coils Q-factors at 6.78 MHz

Coil name	Simulated Q	Measured Q
Coil 1	70	37
Coil 2	69	37
Coil 3	74	47
Coil 4	81	52
Coil 5	85	65
Coil 6	88	65
Coil 7	95	81
Coil 8	100	80
Coil 9	108	75
Coil T/R	351	227

The Q-factor of the spiraled resonating coils $L_{T/R}$ in this work is compared with other coils reported in the literature and shown in Table 3.2. The Q-factor of the coil defines the loss in the system and affects the PTE of WPT. The efficiency of the system depends on the Q-factor, which can be determined by exchanging the resistance of coils R with the expression $R = \omega L/Q$ in the eq.-s (3.9) and (3.15), for three-coil and four-coil WPT systems, respectively.

Table 3.2: Q-factor of resonator coils in other works

Q-factor	Diameter, cm	Operation Frequency, MHz	Reference
418	68.0	13.56	[38]
274	12.0	6.78	[39]
201	23.5	6.78	[44]
45	3.0	6.78	[45]
178	11.3	6.78	[46]
227	18.0	6.78	Article V

3.8 Control circuitry for the interspiraled coils

The control system for the adaptive inductive IMN requires current tracker circuitry on the Tx side. The measured current value helps to estimate impedance mismatch in the system. It then can be used to decide which interspiraled coils can be activated. The block diagram of such a

system is presented in Fig. 3.26. A micro-control unit (MCU) is used for the activation/deactivation of switches, which connects interspiraled coils to the power source.

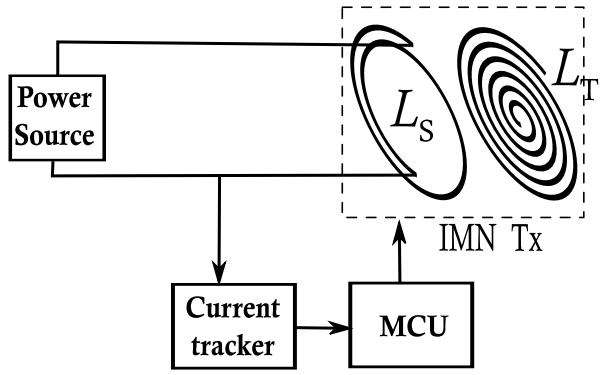

Figure 3.26: Block diagram of control system for adaptive IMN at Tx side.

This automated coil selection can be executed using relays which can be controlled by a micro-controller. A 16-channel USB Relay Module from SainSmart in Fig. 3.27 can be used for this purpose. The relays on the board will add contact-resistance to the coils and decrease the Q-factor. The contacts of relays are often made of silver alloys with a contact resistance normally below $100m\Omega$, which is comparable with the resistance of coils. Another option is the solid-state relays. These have normally higher on-resistance starting from $100m\Omega$. The main advantage of solid-state relays is that their contact point don't wear out, and the contact resistance will remain constant over time.

The process of choosing the correct coil for optimizing PTE is time-consuming due to the optimization calculations required. This becomes even more complicated if there is a continuous distance change or variation in misalignment. Therefore, an effective algorithm for choosing the optimal coil must be developed such as in [24], [28] and [47]. [47] presents a method on the basis of measuring the return loss S_{11} of the system for choosing the optimal coil. The algorithm sweeps between all the coils and chooses the coil that gives the lowest S_{11}. The same principle has been used in [24] for capacitive impedance matching. In [28] three other algorithms are presented for finding the optimal matching based on current measurement to find the optimal impedance. They also present a method referred to as Effective Window Prediction (EWP) search, which

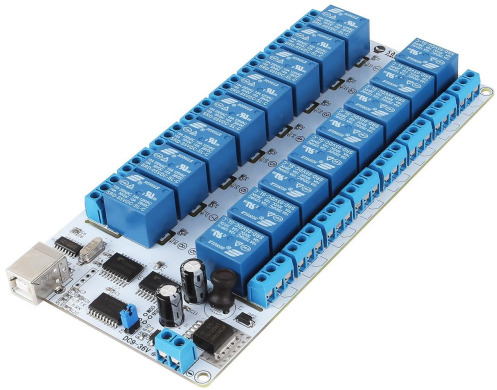

Figure 3.27: A 16 channel USB Relay Module for automatically controlling the coils.

may reduce the timing of the search for optimal selection of capacitors. Even though the algorithms presented in [28] are designed for a capacitive matching network, they can be easily adapted to the inductive methods discussed and presented in this paper.

Connections between the switches, coils, and power source require traces at the backside of the PCB. These traces will act as parasitic capacitances and inductors. It is well-known that the shape and position of the traces on the backside will affect the properties of coils [48, 49]. In [49] the mutual inductance of coils on the backside is used to tune one inductor. This method of tuning results in a lowering of quality factor. We analyzed the effects of the traces on Q-factors of coils. For this reason, different traces are placed at the backside of the PCB and simulated in the Comsol Multiphysics environment as shown in Fig. 3.28. Two types of traces are investigated closely: circles and straight lines.

As expected, the circle trace has more effect on the self-inductance of the interspiraled coils compared to straight traces. The self-inductance of the interspiraled coil 5 and 9 is decreased by about 40 nH and 60 nH because of mutual coupling with the circle trace. On the other hand, the straight traces have less effect on the self-inductance of coils, however, Q-factors of coils are still reduced significantly due to eddy currents. For instance, for interspiraled coils 5 and 9, ohmic losses are increased from 0.13 Ω to 0.53 Ω and 0.2 Ω to 1.2 Ω, respectively. Therefore, it has a huge impact on the efficiency of our system. To avoid this a shielding between traces and coils is required to minimize their effect. There is an option of making shielding as described in [50] or implementing circuitry

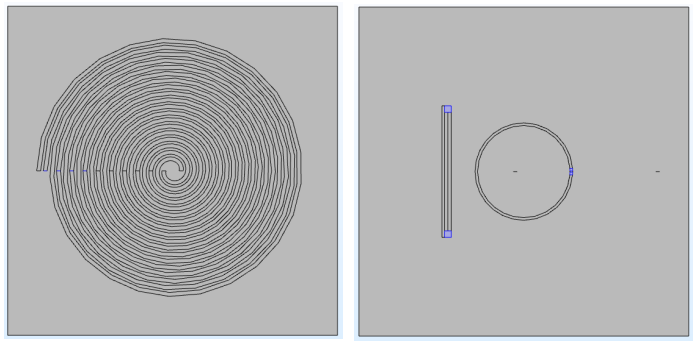

Figure 3.28: Simulated structure in COMSOL Multiphysics: interspiraled coils on frontside of PCB and traces straight and circle traces on backside of PCB.

on another PCB and connecting to coils using pins, which is also in plans for future work.

4 Conclusion

This PhD thesis discussed the impedance matching network (IMN), emphasizing the inductive method for magnetic resonant wireless power transfer systems. IMN is a key factor for improving power transfer efficiency, which is highly sensitive to distance changes and misalignment between the transmitter and the receiver coils.

We started the thesis with a brief introduction to wireless power transfer (WPT) systems and gave an overview of the current IMN methods used in inductive wireless power transfer systems. We proposed a method for comparison of the performance of two popular impedance matching techniques, namely capacitive and inductive IMNs which are presented in Articles I and III. Smith charts are used to visualize the matchable regions offered by these methods. For this study, three different applications were considered with constraints: case A – car charging operating at 85 kHz, case B – mobile phone charging at 6.78 MHz, and case C, a high-frequency charging device at 100 MHz.

The first part of this PhD was dedicated to studying the inductive IMN and its comparison to the capacitive method in WPT systems as there was a lack of research in this field. From the comparison research, we concluded that the inductive IMN can be very effective for the compensation of distance changes between resonator coils. Therefore, two different, new methods of inductive IMN were proposed based on switchable inductors and interspiraled coils. Both methods offer a compact design and can be implemented on PCB.

A switchable coil with ten loops and a high Q-factor resonant coil was designed on opposite sides of the same 2-sided PCB. In this case, the self-inductance of the switchable coil varied from 19 nH to 373 nH at 6.78 MHz with an almost linear behavior, whereas the inductance of the high-Q resonant coil was 9.6 μH. The simulation of mutual inductance between the switchable and the high-Q coils was verified by measurement results, which give an almost linear increase in the range of 25-1230 nH.

The subsequent developed interspiraled coils were even more compact and allowed the whole system, including the coil and electronic circuitry, to be placed on a two-sided PCB. The change in mutual inductance between the driving coils and the resonating coil was linear between 28-1021 nH, which is verified by COMSOL simulations and measurements.

During the PhD, we performed an in-depth study of matching using inductive IMN with interspiraled coils and demonstrated an improvement

of the PTE over a range of distances from 7 to 25 cm through measurements of a full-functioning WPT system with the proposed interspiraled coils.

4.1 Future work

Due to the limited duration of the PhD many ideas have not been explored, and experiments and research were not conducted. Future work should be focused on both further analysis and development of the inductive IMN based on interspiraled coils:

- Studying different combinations of interspiraled coils for further improvement of the PTE for two-side (Tx and Rx) impedance matching.

- Developing a control system for automatic activation of coils for different scenarios.

- Developing a sensing system, such as a current sensor on the receiver or transmitter side for monitoring the impedance change.

- Establishing a more sophisticated experimental setup and methodology.

- Implementing shielding from the circuitry of the control system

References

[1] A. Alphones and P. Jayathurathnage. "Review on wireless power transfer technology (invited paper)". In: *2017 IEEE Asia Pacific Microwave Conference (APMC)*. Nov. 2017, pp. 326–329. DOI: 10.1109/APMC.2017.8251445.

[2] D. L. Sengupta and T. K. Sarkar. "Maxwell, Hertz, the Maxwellians, and the early history of electromagnetic waves". In: *IEEE Antennas and Propagation Magazine* 45.2 (2003), pp. 13–19.

[3] A. S. Marincic. "Nikola Tesla and the Wireless Transmission of Energy". In: *IEEE Transactions on Power Apparatus and Systems* PAS-101.10 (1982), pp. 4064–4068.

[4] H. Hu et al. "A system of two piezoelectric transducers and a storage circuit for wireless energy transmission through a thin metal wall". In: *IEEE Transactions on Ultrasonics, Ferroelectrics, and Frequency Control* 55.10 (Oct. 2008), pp. 2312–2319. ISSN: 0885-3010. DOI: 10.1109/TUFFC.930.

[5] Y. Gibbs at NASA. *Beamed Laser Power for UAVs*. 2003.

[6] C. Hu et al. "One- and two-dimensional antenna arrays for microwave wireless power transfer (MWPT) systems". In: *2017 IEEE Wireless Power Transfer Conference (WPTC)*. May 2017, pp. 1–5. DOI: 10.1109/WPT.2017.7953903.

[7] J. A. G. Akkermans et al. "Analytical models for low-power rectenna design". In: *IEEE Antennas and Wireless Propagation Letters* 4 (2005), pp. 187–190. ISSN: 1536-1225. DOI: 10.1109/LAWP.2005.850798.

[8] A. Sample and J. R. Smith. "Experimental results with two wireless power transfer systems". In: *2009 IEEE Radio and Wireless Symposium*. 2009, pp. 16–18.

[9] F. Lu, H. Zhang, and C. Mi. "A review on the recent development of capacitive wireless power transfer technology". In: *Energies* 10.11 (2017), p. 1752.

[10] P. Basset et al. "Complete System for Wireless Powering and Remote Control of Electrostatic Actuators by Inductive Coupling". In: *IEEE/ASME Transactions on Mechatronics* 12.1 (Feb. 2007), pp. 23–31. ISSN: 1083-4435. DOI: 10.1109/TMECH.2006.886245.

[11] J. Gao. "Traveling Magnetic Field for Homogeneous Wireless Power Transmission". In: *IEEE Transactions on Power Delivery* 22.1 (Jan. 2007), pp. 507–514. ISSN: 0885-8977. DOI: 10.1109/TPWRD.2006.876645.

[12] A. Kurs et al. "Wireless power transfer via strongly coupled magnetic resonances". In: *science* 317.5834 (2007), pp. 83–86.

[13] A. Karalis, J. D. Joannopoulos, and M. Soljačić. "Efficient wireless non-radiative mid-range energy transfer". In: *Annals of physics* 323.1 (2008), pp. 34–48.

[14] K. Y. Kim. *Wireless power transfer-principles and engineering explorations*. intechopen, 2012.

[15] J. Kim, D. H. Kim, and Y. J. Park. "Analysis of capacitive impedance matching networks for simultaneous wireless power transfer to multiple devices". In: *IEEE Transactions on Industrial Electronics* 62.5 (2015), pp. 2807–2813.

[16] Amir Babaki, Sadegh Vaez-Zadeh, and Ali Zakerian. "Performance Optimization of Dynamic Wireless EV Charger Under Varying Driving Conditions Without Resonant Information". In: *IEEE Transactions on Vehicular Technology* 68.11 (2019), pp. 10429–10438. DOI: 10.1109/TVT.2019.2944153.

[17] Reza Tavakoli and Zeljko Pantic. "Analysis, Design, and Demonstration of a 25-kW Dynamic Wireless Charging System for Roadway Electric Vehicles". In: *IEEE Journal of Emerging and Selected Topics in Power Electronics* 6.3 (2018), pp. 1378–1393. DOI: 10.1109/JESTPE.2017.2761763.

[18] Hao Feng et al. "Advances in High-Power Wireless Charging Systems: Overview and Design Considerations". In: *IEEE Transactions on Transportation Electrification* 6.3 (2020), pp. 886–919. DOI: 10.1109/TTE.2020.3012543.

[19] A. P. Sample, D. T. Meyer, and J. R. Smith. "Analysis, experimental results, and range adaptation of magnetically coupled resonators for wireless power transfer". In: *IEEE Transactions on industrial electronics* 58.2 (2011), pp. 544–554.

[20] A. P. Sample et al. "Enabling Seamless Wireless Power Delivery in Dynamic Environments". In: *Proceedings of the IEEE* 101.6 (2013), pp. 1343–1358.

[21] C. J. Chen, T. H. Chu, and Z. C. Lin C. L.and Jou. "A study of loosely coupled coils for wireless power transfer". In: *IEEE Transactions on Circuits and Systems II: Express Briefs* 57.7 (2010), pp. 536–540.

[22] J. Kim et al. "Coil design and shielding methods for a magnetic resonant wireless power transfer system". In: *Proceedings of the IEEE* 101.6 (2013), pp. 1332–1342.

[23] M. Kesler. "Highly resonant wireless power transfer: safe, efficient, and over distance". In: *Witricity corporation* (2013), pp. 1–32.

[24] T. C. Beh et al. "Automated Impedance Matching System for Robust Wireless Power Transfer via Magnetic Resonance Coupling". In: *IEEE Transactions on Industrial Electronics* 60.9 (2013), pp. 3689–3698.

[25] Z. Wang, S. Gao, and C. W. Park. "A simple method for tunable load impedance matching network of power amplifier". In: *2010 International Conference on Microwave and Millimeter Wave Technology*. IEEE. 2010, pp. 484–487.

[26] B. K. Eplett. *On-chip impedance matching using a variable capacitor*. US Patent App. 11/680,644. Sept. 2008.

[27] W. S. Lee et al. "Switchable distance-based impedance matching networks for a tunable HF system". In: *Progress in Electromagnetics Research-Pier* 128 (2012), pp. 19–34.

[28] Y. Lim et al. "An adaptive impedance-matching network based on a novel capacitor matrix for wireless power transfer". In: *IEEE Transactions on Power Electronics* 29.8 (2014), pp. 4403–4413.

[29] K. A. Grajski, R. Tseng, and C. Wheatley. "Loosely-coupled wireless power transfer: Physics, circuits, standards". In: *2012 IEEE MTT-S International Microwave Workshop Series on Innovative Wireless Power Transmission: Technologies, Systems, and Applications*. 2012, pp. 9–14.

[30] M. Treffers. "History, Current Status and Future of the Wireless Power Consortium and the Qi Interface Specification". In: *IEEE Circuits and Systems Magazine* 15.2 (2015), pp. 28–31.

[31] L. Chen et al. "An Optimizable Circuit Structure for High-Efficiency Wireless Power Transfer". In: *IEEE Transactions on Industrial Electronics* 60.1 (2013), pp. 339–349.

[32] J. Lee et al. "Wireless Power Transfer System Adaptive to Change in Coil Separation". In: *IEEE Transactions on Antennas and Propagation* 62.2 (2014), pp. 889–897.

[33] Q. Wang et al. "Conjugate image impedance matching for maximizing the gains of a WPT link". In: *2018 IEEE MTT-S International Wireless Symposium (IWS)*. 2018, pp. 1–3.

[34] Marco Dionigi, Mauro Mongiardo, and Renzo Perfetti. "Rigorous Network and Full-Wave Electromagnetic Modeling of Wireless Power Transfer Links". In: *IEEE Transactions on Microwave Theory and Techniques* 63.1 (2015), pp. 65–75. DOI: 10.1109/TMTT.2014.2376555.

[35] S. Roberts. "Conjugate-Image Impedances". In: *Proceedings of the IRE* 34.4 (1946), 198p–204p.

[36] S. Cheon et al. "Circuit-Model-Based Analysis of a Wireless Energy-Transfer System via Coupled Magnetic Resonances". In: *IEEE Transactions on Industrial Electronics* 58.7 (2011), pp. 2906–2914.

[37] J. Kim and J. Jeong. "Range-adaptive wireless power transfer using multiloop and tunable matching techniques". In: *IEEE Transactions on Industrial Electronics* 62.10 (2015), pp. 6233–6241.

[38] J. Kim, W.S. Choi, and J. Jeong. "Loop Switching Technique for Wireless Power Transfer Using Magnetic Resonance Coupling". In: *Progress In Electromagnetics Research)* 138 (2013), pp. 197–209.

[39] B. Park and J. Lee. "Adaptive Impedance Matching of Wireless Power Transmission Using Multi-Loop Feed With Single Operating Frequency". In: *IEEE Transactions on Antennas and Propagation* 62.5 (2014), pp. 2851–2856.

[40] Y. Chen et al. "Hybrid Topology With Configurable Charge Current and Charge Voltage Output-Based WPT Charger for Massive Electric Bicycles". In: *IEEE Journal of Emerging and Selected Topics in Power Electronics* 6.3 (2018), pp. 1581–1594.

[41] Vijith Vijayakumaran Nair and Jun Rim Choi. "An efficiency enhancement technique for a wireless power transmission system based on a multiple coil switching technique". In: *Energies* 9.3 (2016), p. 156.

[42] N. S. Jeong and F. Carobolante. "Enabling wireless power transfer though a metal encased handheld device". In: *2016 IEEE Wireless Power Transfer Conference (WPTC)*. 2016, pp. 1–3. DOI: 10.1109/WPT.2016.7498817.

[43] S. Chen, Y. Yang, and Y. Luo. "Comparison of spiral and helix coils in magnetic resonant coupling wireless power transfer". In: *2017 IEEE 2nd Information Technology, Networking, Electronic and Automation Control Conference (ITNEC)*. 2017, pp. 721–724. DOI: 10.1109/ITNEC.2017.8284826.

[44] C. Florian et al. "Theoretical and Numerical Design of a Wireless Power Transmission Link With GaN-Based Transmitter and Adaptive Receiver". In: *IEEE Transactions on Microwave Theory and Techniques* 62.4 (2014), pp. 931–946. DOI: 10.1109/TMTT.2014.2303949.

[45] A. Khripkov, W. Hong, and K. Pavlov. "Design of an integrated resonant structure for wireless power transfer and data telemetry". In: *2013 IEEE MTT-S International Microwave Workshop Series on RF and Wireless Technologies for Biomedical and Healthcare Applications (IMWS-BIO)*. 2013, pp. 1–3. DOI: 10.1109/IMWS-BIO.2013.6756137.

[46] M. Liu, M. Fu, and C. Ma. "Low-Harmonic-Contents and High-Efficiency Class E Full-Wave Current-Driven Rectifier for Megahertz Wireless Power Transfer Systems". In: *IEEE Transactions on Power Electronics* 32.2 (2017), pp. 1198–1209. DOI: 10.1109/TPEL.2016.2551288.

[47] Jungsik Kim and Jinho Jeong. "Range-Adaptive Wireless Power Transfer Using Multiloop and Tunable Matching Techniques". In: *IEEE Transactions on Industrial Electronics* 62.10 (2015), pp. 6233–6241. DOI: 10.1109/TIE.2015.2420041.

[48] Yang Chen, Guozhu Chen, and K. Smedley. "Analysis and measurement of small inductance of loops and vias on printed circuit board". In: 2 (2003), 1661–1666 Vol.2. DOI: 10.1109/IECON.2003.1280307.

[49] Mina Rais-Zadeh, Paul A. Kohl, and Farrokh Ayazi. "MEMS Switched Tunable Inductors". In: *Journal of Microelectromechanical Systems* 17.1 (2008), pp. 78–84. DOI: 10.1109/JMEMS.2007.910257.

[50] S.C. Tang, S.Y. Hui, and H.S.-H. Chung. "Evaluation of the shielding effects on printed-circuit-board transformers using ferrite plates and copper sheets". In: *IEEE Transactions on Power Electronics* 17.6 (2002), pp. 1080–1088. DOI: 10.1109/TPEL.2002.805585.

Article I

Y. Zhaksylyk and M. Azadmehr, "Comparative Analysis of Inductive and Capacitive Feeding of Magnetic Resonance Wireless Power Transfer," 2018 IEEE PELS Workshop on Emerging Technologies: Wireless Power Transfer (Wow), Montréal, QC, 2018, pp. 1-5, doi: 10.1109/WoW.2018.8450891.

Article II

Y. Zhaksylyk, U. Hanke and M. Azadmehr, "Design of a switchable driving coil for Magnetic Resonance Wireless Power Transfer," 2019 IEEE PELS Workshop on Emerging Technologies: Wireless Power Transfer (WoW), London, United Kingdom, 2019, pp. 249-252,
doi: 10.1109/WoW45936.2019.9030674.

Article III

Y. Zhaksylyk, E. Halvorsen, U. Hanke, and M. Azadmehr, "Analysis of Fundamental Differences between Capacitive and Inductive Impedance Matching for Inductive Wireless Power Transfer", Electronics 2020, 9, 476, doi: 10.3390/electronics9030476

electronics

MDPI

Article

Analysis of Fundamental Differences between Capacitive and Inductive Impedance Matching for Inductive Wireless Power Transfer

Yelzhas Zhaksylyk *, Einar Halvorsen, Ulrik Hanke and Mehdi Azadmehr

Department of Microsystems, University of South-Eastern Norway, Campus Vestfold, NO-3184 Horten, Norway; Einar.Halvorsen@usn.no (E.H.); Ulrik.Hanke@usn.no (U.H.); Mehdi.Azadmehr@usn.no (M.A.)

* Correspondence: Yelzhas.Zhaksylyk@usn.no

Received: 21 February 2020; Accepted: 6 March 2020; Published: 13 March 2020

Abstract: Inductive and capacitive impedance matching are two different techniques optimizing power transfer in magnetic resonance inductive wireless power transfer. Under ideal conditions, i.e., unrestricted parameter ranges and no loss, both approaches can provide the perfect match. Comparing these two techniques under non-ideal conditions, to explore fundamental differences in their performance, is a challenging task as the two techniques are fundamentally different in operation. In this paper, we accomplish such a comparison by determining matchable impedances achievable by these networks and visualizing them as regions of a Smith chart. The analysis is performed over realistic constraints on parameters of three different application cases both with and without loss accounted for. While the analysis confirms that it is possible to achieve unit power transfer efficiency with both approaches in the lossless case, we find that the impedance regions where this is possible, as visualized in the Smith chart, differ between the two approaches and between the applications. Furthermore, an analysis of the lossy case shows that the degradation of the power transfer efficiencies upon introduction of parasitic losses is similar for the two methods.

Keywords: impedance matching network; parasitic resistance; power loss; reflection coefficient; Smith chart; wireless power transfer

1. Introduction

Recent demand on mobility and accessibility of devices is pushing the development of wireless technology to new levels. There are good solutions for data transfer such as WiFi and Bluetooth, whereas, power is still delivered by either batteries or cable, the main bottleneck in the strive for cutting all the wires and limiting the mobility of devices.

For daily-life applications, inductive wireless power transmission has drawn increasing attention from researchers as it offers the highest power transfer efficiency (PTE) among other alternatives such as capacitive, microwave, laser, and acoustic [1,2]. Various products such as electric toothbrushes and mobile chargers using this technique are already commercially available. This technique provides two advantages compared to others: transfer of high power and low-frequency operation, making it less hazardous to the human body [3]. The main issue with this type of inductive wireless power transfer (WPT) is the mobility as the sender and receiver need to be close to each other, less than a few centimetres. Magnetic resonant (MR) WPT, an inductive technique based on highly coupled high-Q resonators, addresses this issue and offers a reasonable distance of power transfer (up to 2 m) [4]. However, a considerable challenge of MR-WPT is to maintain high power transfer throughout a range of distances between resonators and for variations in load value, as these will cause a mismatch between the source and input impedances [5].

Electronics **2020**, *9*, 476

In order to solve this challenge, different types of impedance matching techniques have been developed in the last decades. The simplest and most popular ones use capacitive or inductive impedance matching networks (IMNs). The capacitive method uses variable capacitors to tune the transmitter to the resonant frequency or a predefined capacitor sequence for different distances [6,7]. There is a variety of adaptive frequency tuning systems where L, T and Π-type impedance matching networks contain capacitors [7,8]. Matching can potentially also provide power to multiple device WPT by using only a single transmitter [9].

The four-coil MR-WPT system presented by the MIT group in 2007 [4] has become a recognized solution [10–14] for highly resonant WPT systems for medium distances. The system consists of two or more high-Q resonating coils which are driven by a low-Q coil connected to the power source. The load is also connected to a low-Q coil. The coupling between resonator and the driver coils (or the load coil) can be considered as parts of a matching network, where tuning of the impedance can be achieved by changing the coupling between them. In our study, this method is referred to as inductive matching. In a previous work, we showed that these two matching techniques, i.e., the capacitive and inductive matching could potentially achieve a similar level of matching in certain cases [15]. Among the many different capacitive compensation circuitries, we chose the parallel-series compensation according to reference [8] for comparison to the inductive method. This network offers sufficient degrees of freedom to match perfectly if there is no loss and no restriction on parameter ranges, hence it is sufficient to give an insight into the effect of these limitations. The presented comparison method can also be used to identify matchable regions of other compensation structures.

The aforementioned matching techniques, i.e., capacitive and inductive can be applied to any mismatches in a WPT system to improve the power transfer efficiency [16]. However, there is a challenge in the direct comparison of their matching performances because they have different circuit topologies. The paper describes a method that makes a systematic comparison of their performance possible. The proposed method is based on comparison of the conjugate impedance of the matchable load, displayed in the Smith chart. The conjugate matching method has been analysed in [17], where all concepts of conservation and amplification of power by two port network was defined. This method is used by [18,19] to describe efficiency of the WPT system with inductive IMN. Our work presents a comparison of the matchable loads offered by the inductive and capacitive matching networks over a full range of realistic parameter ranges for three different applications distinguished by their operating frequency and power level [20–22]. The operating frequencies are within the allowed Industrial, Scientific and Medical (ISM) bands [9], which also limits the frequency range in the analysis. For the ease of simulation and calculations we choose to keep the distance constant and match the different load values. We assume the coil sizes are such that the systems operate in near field and the inductances of sender and receiver coils are equal, as in the [18–22].

This paper is organized as follows. In Section 2, impedances are analysed by derivation of reflection coefficients. We intentionally exclude the parasitic components in the system in order to have a clear comparison between these matching techniques in the ideal case. Subsequently, Section 3 visualizes the matchable reflection coefficients in the Smith chart, which graphically illustrates all of the possible complex impedances that are obtained by sweeping matching parameters. Therefore, it demonstrates which method offers the wider area of impedances that can be matched. Furthermore, the impact of parasitic loss to the matchable region is analyzed and optimized power simulation is given in the Section 4 and Section 5 discusses the outcome of the comparison.

2. Reflection Coefficients

In order to map and compare the tunable impedances of WPT systems, suitable circuit models and corresponding impedance expressions should be established. A generic WPT system with impedance matching networks can be represented as shown in Figure 1. The driving source consists of an ideal voltage source (V_S) and a series resistance R_S. The two-port network consists of resonators, and here

we will consider capacitive and inductive impedance matching circuits. The network is terminated by load impedance Z_L at the output. Here, i_S and i_L are currents through R_S and Z_L, respectively.

Matching networks are necessary to obtain a match between input impedance Z_{in} and source impedance R_S. They affect the Power Transfer Efficiency (PTE), defined as ratio between power delivered to the load and input power of the two-port network [18]. This research focuses on the comparison of the matchable loads offered by the capacitive and inductive IMNs. Therefore, the two-port network is redrawn as in Figure 2 to get value of an effective impedance Z_{out} at the output, which is a complex conjugate Z_L^* form of load impedance that can be perfectly matched.

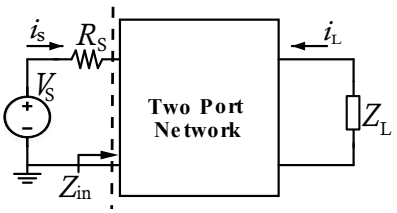

Figure 1. Two-port network representation of a highly resonant WPT system.

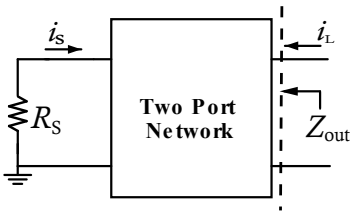

Figure 2. Two-port network representation when source is terminated.

2.1. Capacitive Matching Network

A lossless model of the inductive resonant WPT system with capacitive impedance matching is shown in Figure 3. The circuit elements are ideal, i.e., inductors and capacitors do not have parasitics. Matching networks consist of series-parallel connection of capacitors C_{ts}, C_{tp} and C_{rp}, C_{rs} at the transmitter (Tx) and receiver (Rx) sides. The source impedance is considered as resistance R_S.

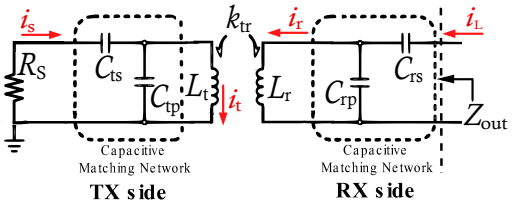

Figure 3. Equivalent circuit of a WPT system with capacitive impedance matching network.

Applying Kirchhoff's voltage law (KVL) to the circuit in Figure 3, the voltage-current relations can be written in an impedance matrix form

$$\begin{bmatrix} V_{out} \\ 0 \\ 0 \\ 0 \end{bmatrix} = \begin{bmatrix} Z_{11} & Z_{12} & 0 & 0 \\ Z_{21} & Z_{22} & Z_{23} & 0 \\ 0 & Z_{32} & Z_{33} & Z_{34} \\ 0 & 0 & Z_{43} & Z_{44} \end{bmatrix} \begin{bmatrix} i_L \\ i_r \\ i_t \\ i_S \end{bmatrix} \tag{1}$$

where

$$Z_{11} = \frac{1}{j\omega C_{rs}} + \frac{1}{j\omega C_{rp}},\ Z_{12} = -\frac{1}{j\omega C_{rp}}, \tag{2}$$

$$Z_{21} = -\frac{1}{j\omega C_{rp}},\ Z_{22} = j\omega L_r + \frac{1}{j\omega C_{rp}},\ Z_{23} = j\omega M_{12}, \tag{3}$$

$$Z_{32} = j\omega M_{tr}, Z_{33} = j\omega L_t + \frac{1}{j\omega C_{tp}}, Z_{34} = -\frac{1}{j\omega C_{tp}}, \tag{4}$$

$$Z_{43} = -\frac{1}{j\omega C_{tp}},\ Z_{44} = R_S + \frac{1}{j\omega C_{ts}} + \frac{1}{j\omega C_{tp}}. \tag{5}$$

Here,

$$M_{tr} = k_{tr}\sqrt{L_t L_r},\ \ 0 \le k_{tr} \le 1 \tag{6}$$

is the mutual inductance between inductors L_t and L_r. The coefficient k_{tr} represents the coupling between them and its value is inversely proportional to the cube of their distance [15]. The distance change and variation of load impedance can be controlled by adjusting the capacitances C_{ts}, C_{tp} and C_{rs}, C_{rp} in the matching networks.

The effective impedance Z_{out} at the output of two-port network is

$$Z_{\text{out}} = jX_r + \frac{Z_{12}^2(Z_{34}^2 - Z_{33}Z_{44})}{(Z_{22}Z_{33} - Z_{32}^2)Z_{44} - Z_{34}^2 Z_{22}}, \tag{7}$$

where

$$X_r = -\frac{1}{\omega C_{rs}} - \frac{1}{\omega C_{rp}}. \tag{8}$$

The real and imaginary parts of the impedance are

$$Re\{Z_{\text{out}}\} = \Delta R_S,\ Im\{Z_{\text{out}}\} = \Delta A - \frac{1}{\omega C_{rs}} - \frac{1}{\omega C_{rp}}, \tag{9}$$

where

$$\Delta = \frac{\omega^2 M_{tr}^2 Z_{12}^2 Z_{34}^2}{B^2 R_S^2 + (X_t B - Z_{34}^2 Z_{22})^2}, \tag{10}$$

$$B = Z_{22}Z_{33} - Z_{32}^2,\ X_t = -\frac{1}{\omega C_{ts}} - \frac{1}{\omega C_{tp}}, \tag{11}$$

$$A = \frac{(Z_{22}Z_{34}^2 - X_t\omega^2 M_{tr}^2)Z_{34}^2 - Z_{33}B(X_t^2 + R_S^2)}{\omega^2 M_{tr}^2 Z_{34}^2}. \tag{12}$$

The impedance Z_{out} can be seen at the output of the two-port network, which is complex conjugate form of load impedance Z_L. This impedance is used to derive the reflection coefficient (Γ), which can be seen from the load side

$$\Gamma = (Z_{\text{out}} - Z_0)/(Z_{\text{out}} + Z_0) \tag{13}$$

where Z_0 is reference impedance equal to R_S.

Equation (13) is used to draw Γ in the Smith chart to visualize graphically and estimate the values of load impedance that can be perfectly matched. Furthermore, a derivation of the reflection coefficient expression for the inductive matching is discussed in next section, and numerical results are given in Section 3.

2.2. Inductive Matching Network

Inductive coupling is another method widely exploited to match the input impedance for different distances between resonators or load variation. This system uses additional magnetically coupled

coils at the transmitter or receiver, or both, to enhance the PTE. These coils do not need as high Q as the resonator coils. The most popular one is a four-coils system with source coil L_S, high-Q transmitter coil L_t, high-Q receiver coil L_r, and load coil L_L [4,15]. The matching can be controlled by varying couplings between the source/load coils and high-Q coils—k_S, k_L. The equivalent lossless model of such a system is shown in Figure 4. The high-Q coils are connected to series external capacitors to form resonators.

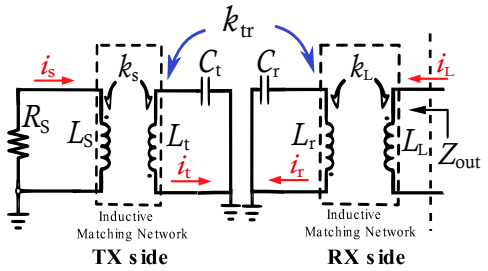

Figure 4. Equivalent circuit of WPT system with inductance matching network.

For such a circuit, the same voltage-current relations can be used as in Equation (1), where impedances are

$$Z_{11} = j\omega L_L,\ Z_{12} = -j\omega M_L, \tag{14}$$

$$Z_{21} = -j\omega M_L, Z_{22} = j\omega L_t + \frac{1}{j\omega C_t}, Z_{23} = j\omega M_{tr}, \tag{15}$$

$$Z_{32} = j\omega M_{tr}, Z_{33} = j\omega L_r + \frac{1}{j\omega C_r}, Z_{34} = -j\omega M_S, \tag{16}$$

$$Z_{43} = -j\omega M_S,\ Z_{44} = R_S + j\omega L_S, \tag{17}$$

and by neglecting cross-coupling:

$$Z_{13} = Z_{14} = Z_{24} = Z_{31} = Z_{41} = Z_{42} = 0. \tag{18}$$

Here, $M_{S/L}$ is a mutual inductance between source/load coil ($L_{S/L}$) and high-Q coil ($L_{t/r}$)

$$M_{S/L} = k_{S/L}\sqrt{L_{S/L}L_{t/r}},\ \ 0 \le k_{S/L} \le 1. \tag{19}$$

and M_{tr} is the mutual inductance between resonator coils

$$M_{tr} = k_{tr}\sqrt{L_t L_r},\ \ 0 \le k_{tr} \le 1. \tag{20}$$

If we assume that the two resonators have same resonance frequency $\omega = 1/\sqrt{L_{t/r}C_{t/r}}$, then

$$Z_{22} = Z_{33} = 0. \tag{21}$$

From impedance Equations (14)–(18) the real and imaginary parts of output impedance Z_{out} become

$$Re\{Z_{\text{out}}\} = \Delta R_S,\ Im\{Z_{\text{out}}\} = \omega(L_L - \Delta L_S), \tag{22}$$

where

$$\Delta = \frac{\omega^2 M_S^2 M_L^2}{M_{tr}^2(R_S^2 + \omega^2 L_S^2)}. \tag{23}$$

Electronics **2020**, *9*, 476

Furthermore, Equations (13), (22) and (23) are used to calculate the reflection coefficient in the following section. These results conclude the theoretical analysis that is required to compare the two techniques.

3. Matchable Regions of Lossless Model

This section presents graphs of reflection coefficients in the Smith Chart, based on the equations derived in the previous section for both capacitive and inductive matching. These graphs help us to estimate the matchable loads and to select the proper matching network at the transmitter and receiver side. In the capacitive method the input impedance is controlled via capacitances C_{ts}, C_{tp}, C_{rs}, C_{rp}, whereas in the inductive matching it is controlled by coupling coefficients k_S, k_L between the source/load coils and high-Q coils.

In this section, the parasitic components of the system are intentionally excluded to have a clear and ideal case comparison between these two matching techniques. Reflection coefficients were examined for three specific applications, and parameter values used for the cases given in Table 1. The presented cases have been chosen so that they cover a wide range of WPT applications with different specifications for power level and operating frequency [20–22].

Table 1. Applications and parameters.

Application	Operation Frequency	$L_t = L_r$	$C_t = C_r$	k_{tr}	References
Case A—Car charging	85 kHz	60 µH	58.4 nF	0.01	[20]
Case B—Tablet charging	6.78 MHz	6 µH	91.8 pF	0.01	[21]
Case C—High Frequency	100 MHz	2.5 µH	1.01 pF	0.01	[22]

Figures 5–10 show the realizable reflection coefficient values in the Smith Chart. The matchable regions are indicated by bold black borders. Each figure consists of three impedance regions, where each region corresponds to different resulting impedances in the circuit: Z_{tx}—impedance at the transmitter, Z_{tr}—impedance after transmission, Z_{out}—impedance at the output. They are obtained by sweeping the impedance matching network parameters over the realistic range of values, which are given in Table 2. Chosen constraint for the inductive IMN is based on an assumption that the driving and load loops have an inductance equal or smaller than the resonator inductances [4]. The bottom limit for the capacitance variance in the capacitive IMN is the lowest value of capacitance in the market, which is approximately 500 fF (ignoring the possibilities of series connection), whereas the upper limit was chosen sufficient for the application choice. As we can see further from the results the upper limit in the inductive method and lower limit in the capacitive method decides the final shape in the Smith chart. The circuits are equivalent models of an inductive WPT, which consists of source resistance R_S, matching networks (capacitive or inductive), and lossless coils for transmission and reception.

Case A application in Table 1 is an Electric Vehicle (EV) charging station for transmission of high power. It is designed for low-frequency operation, in our case at 85 kHz frequency, and designed for coils around $L_t = L_r = 60$ µH. Figure 5a shows the impedance at the transmitter. This impedance region agrees well with known results for L-type networks in [23]. It is controlled by varying the capacitances C_{ts} and C_{tp} within the range given in Table 2. Since the L-type capacitive matching network at the transmitter (Tx) cannot match all impedances, a matching network is required for the receiver part as well. Second stage, in Figure 5b, illustrates reflection graph after the resonator coils L_t and L_r, which are coupled at $k_{tr} = 0.01$. The inductances change the region into a circle—smaller than Smith chart, which means there is still a limitation in the matchable area. Finally, in Figure 5c, third stage gives impedances that can be matched by the complete network consisting of matching networks at the Tx (C_{ts} and C_{tp}) and Rx (C_{rs} and C_{rp}) sides. All the capacitances in this example are varied from 0.1 pF to 200 pF (Table 2). The impedance matching network at the Rx side greatly improves the matchable area, which now practically fills the Smith chart. It means that for case A

Electronics **2020**, *9*, 476

without losses any load is matchable by the capacitive matching method at $k_{tr} = 0.01$, but it does not mean that this still holds for other coupling coefficient values.

The result of following a similar procedure for case A with the inductive impedance matching network is shown in Figure 6. In this case, matching works by adjusting source/load inductances L_S/L_L and coupling coefficients between these and resonator coils (k_S, k_L). Inductance and coupling constant ranges are given in Table 2. In Figure 6a, we can notice that the inductive method gives an extremely limited region of impedances that can be matched, hence, matching at the receiver becomes crucial. One thing that can be noticed from Figure 6b impedance range of Z_{tr} after the coupling ($k_{tr} = 0.01$) between resonators L_t, L_r is even smaller, and it shows that three-coil system is not suitable for applications where load values are diverse. However, the resulting matchable impedance of the complete system with four coils, where impedance can be matched at both sides (Tx and Rx), fills around 80% of the Smith chart and is shown in Figure 6c. According to the figure, for case A without losses there is roughly 20% of the impedances that cannot be perfectly matched by the inductive approach.

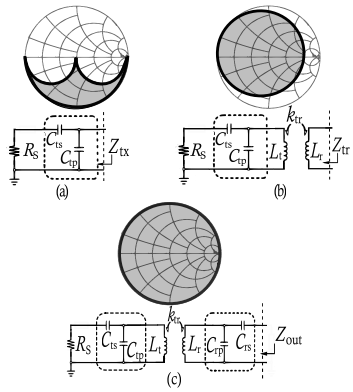

Figure 5. Reflection coefficient graphs show impedances that can be obtained by capacitive matching networks placed into WPT system in case A: (**a**) Z_{tx}—impedance at the transmitter, (**b**) Z_{tr}—impedance after transmission, (**c**) Z_{out}—impedance at the output.

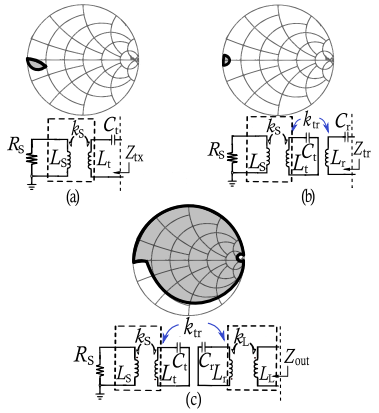

Figure 6. Reflection coefficient graphs show impedances that can be obtained by inductive coupling in four coiled WPT system in case A: (**a**) Z_{tx}—impedance at the transmitter, (**b**) Z_{tr}—impedance after transmission, (**c**) Z_{out}—impedance at the output.

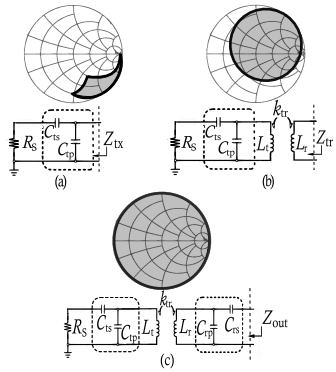

Figure 7. Reflection coefficient graphs show impedances that can be obtained by capacitive matching networks placed into WPT system in case B: (**a**) Z_{tx}—impedance at the transmitter, (**b**) Z_{tr}—impedance after transmission, (**c**) Z_{out}—impedance at the output.

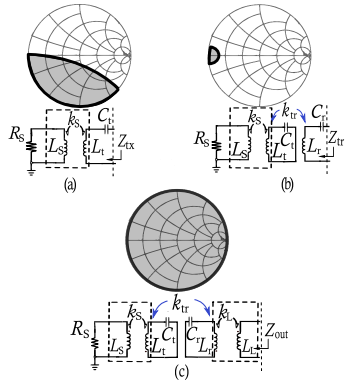

Figure 8. Reflection coefficient graphs show impedances that can be obtained by inductive coupling in four coiled WPT system in case B: (**a**) Z_{tx}—impedance at the transmitter, (**b**) Z_{tr}—impedance after transmission, (**c**) Z_{out}—impedance at the output.

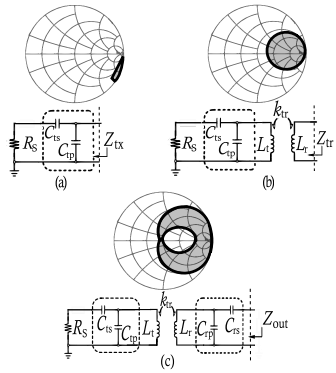

Figure 9. Reflection coefficient graphs show impedances that can be obtained by capacitive matching networks placed into WPT system in case C: (**a**) Z_{tx}—impedance at the transmitter, (**b**) Z_{tr}—impedance after transmission, (**c**) Z_{out}—impedance at the output.

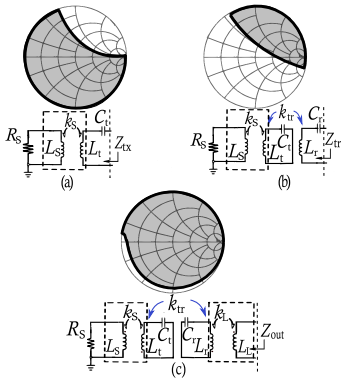

Figure 10. Reflection coefficient graphs show impedances that can be obtained by inductive coupling in four coiled WPT system in case C: (**a**) Z_{tx}—impedance at the transmitter, (**b**) Z_{tr}—impedance after transmission, (**c**) Z_{out}—impedance at the output.

Table 2. Matching network parameters.

Application	L_S, L_L	X_S, X_L	k_S, k_L	$C_{ts/rs}$, $C_{tp/rp}$	$X_{ts/rs}$, $X_{ts/rs}$
Case A	0.1–60 µH	8.5 mΩ–32.0 Ω	0.001–1	0.1–200 nF	187 kΩ–9 Ω
Case B	0.1–6 µH	0.7 Ω–40.7 Ω	0.001–1	0.5–200 pF	47 kΩ–117 Ω
Case C	0.1–2.5 µH	10 Ω–1.6 kΩ	0.001–1	0.5–2 pF	3.2 kΩ–796 Ω

Case B is a low power and high-frequency system, a mobile phone charging device from Airfuel Alliance, which has standard parameters as 6.78 MHz operational frequency and around $L_t = L_r =$ 6 µH coils for Tx and Rx [21]. Results are given in Figures 7 and 8. Here, the inductive method again shows low performance for a three-coil system since the matchable area fills only about 10% of the Smith chart. However, both methods are able to match all loads with the complete network.

Finally, we consider application case C, which is a high-frequency device with $L_t = L_r = 2.5$ µH for Rx and Tx coils. The inductive matching network has larger matchable region than the capacitive method, see Figures 9 and 10. In a complete network, around 90% of the load impedances are matchable by the inductive method, whereas the capacitive approach can match only around 30% of the loads. One thing to note is that the matchable region for the capacitive network has a hole, which appears because of the minimum constraint 0.5 pF in the parameter range. Consequently, the capacitive matching network with these constraints is less versatile in this type of application.

4. Performance of Lossy System

In this section, system performance is examined in the presence of loss. Therefore, the lossless inductors L_t and L_r in the previous circuits is replaced by a model of a non-ideal inductor shown in Figure 11. The model consists of an ideal inductor with a series parasitic resistance and a parallel capacitance. We only consider the effect of the parasitic resistance since the parasitic capacitance can be taken care of by compensation circuits. The parasitic resistance is a combination of ohmic and radiative losses of the coil. Other circuit parameters are kept the same as in the previous section for calculation of reflection coefficients. The realizable reflection coefficients over the chosen range of parameters are shown in Figures 12–14.

The inductances of the coils in case A are larger than for the other two cases, so the parasitic resistance $R = 1$ Ω of each coil is higher than for case B and comparable to case C where the skin effect matters. R is estimated assuming a copper coil made from a 30-m long wire of diameter 0.8 mm [20]. The result for case A is shown in Figure 12, where Figure 12a presents realizable reflection coefficients

Electronics **2020**, *9*, 476

for capacitive IMN of Figures 3 and 12b presents the results for inductive IMN of Figure 4. Solid lines show borders of matchable regions for lossles networks determined in the previous section, whereas dashed lines bound matchable regions for lossy networks.

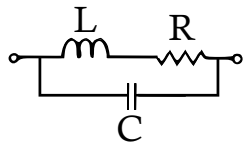

Figure 11. Model of non-ideal inductor.

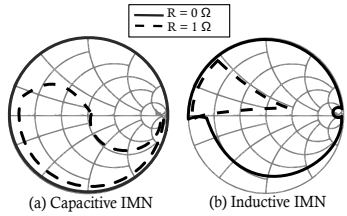

Figure 12. Matchable regions in lossless and lossy model for case A.

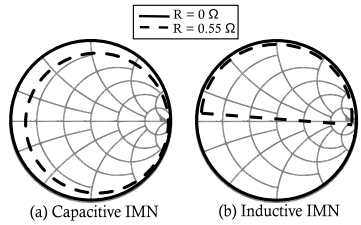

Figure 13. Matchable regions in lossless and lossy model for case B.

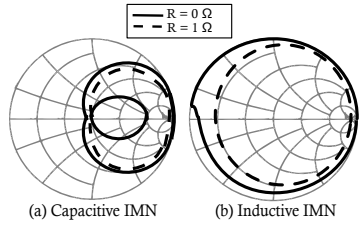

Figure 14. Matchable regions in lossless and lossy model for case C.

The matchable area has been dramatically reduced from 100% to approximately 40% of the Smith chart for capacitive and from 80% to 20% for the inductive technique. It shows that range of matchable impedances is sensitive to loss for both methods and that the inductive method is slightly sensitive to the loss than the capacitive method.

The comparison of matchable regions, after the introduction of parasitic resistance $R = 0.55\ \Omega$ ([21]) in the coils for case B, is shown in Figure 13. The reflection coefficient graphs of capacitive and inductive methods are shown in Figure 13a,b, respectively. The change in the matchable region is again more dramatic for the inductive method since it has about 55% reduction from the ideal case compared to the capacitive method's 20%.

Matchable regions for case C are given in Figure 14. Since the resonator coils operate at the highest frequency in the comparison, we considered skin effect as well. Therefore, ohmic loss at the coils is

Electronics **2020**, *9*, 476

chosen as a combination of parasitic resistance and skin effect loss, which is $R = 1\ \Omega$. R is estimated assuming a copper coil made from a 75-cm long wire of diameter 0.8 mm [22]. As a peculiarity in Figure 14a, we note that the matchable region for the lossless capacitive network has a hole in it and that this vanishes when losses are introduced. The overall numbers are 2% reduction in area for the capacitive and 15% for the inductive approach. While the inductive method in this case still has a matchable region more sensitive to loss than capacitive IMN, the inductive method covers a larger area of matchable impedances both with and without loss.

As mentioned before in Section 2, we considered regions of matchable impedances. It can also be interesting to see how well the network performs for any given load impedance. Here we consider this question by calculating the delivered power to load impedances sampled form the entire Smith chart. It can be obtained in several ways, but we used SPICE AC analysis here. We focused on cases A and B because their matchable regions are most affected by the introduction of ohmic loss. The results are shown in Figures 15 and 16 and demonstrate that capacitive and inductive IMNs can be comparable in matching various load impedances, when the networks are optimized for each particular impedance. Device in case A has more power loss than in case B. Overall, power level is distributed between -4.2 dBm and -4.8 dBm for case A, and -3.5 dBm and -4 dBm for case B.

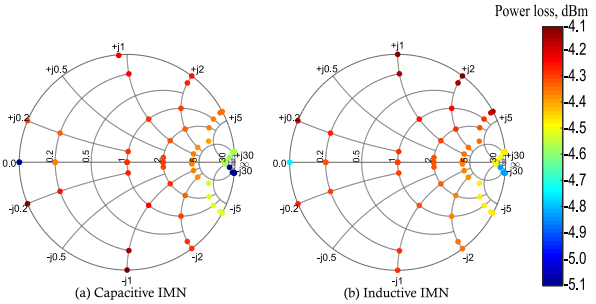

Figure 15. Comparison of optimal power delivered to the various loads for case A.

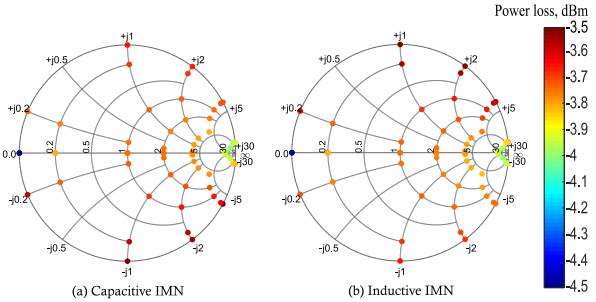

Figure 16. Comparison of optimal power delivered to the various loads for case B.

5. Discussion

Section 3 presented three impedance areas obtained for different stages of ideal circuits (Figures 5–10), which is summarized in Figure 17. In this figure, each trace represents specific application (case A, B, C) and matching network. The impedances at the different stage of circuits, in Figures 5–10, are given in x-axis, whereas y-axis shows a share of Smith chart in percentage. All the areas have been estimated from the graphs. According to the figure, Z_{out} fills a larger area than Z_{tr} for all cases, which shows that the impedance matching network at the Rx side is crucial in obtaining large tunable area of load impedance. There is a degradation from 100 to 30% in the area of output

Electronics **2020**, *9*, 476

impedance Z_{out} by the capacitive method from case A to C. An improvement from 10 to 75% in the area of impedance at the transmitter side Z_{tx} can be seen for the inductive technique from case A to C. This is due to difference in the operation frequency of the specific applications since for capacitive IMN $X_C \propto 1/f$, while for inductive IMN $X_L \propto f$. Therefore, the region of inductive method shrinks in case C (85 kHz—low frequency) and widens in case A (100 MHz—high frequency), and it is vice versa for capacitive matching. At low operation frequencies, the available range of the capacitance values is enough to match most of the load impedances, whereas at high frequency, the matching is limited by the smallest capacitance value in the parameter range, which is 0.5 pF. In the inductive approach, the ranges of load and source inductance values are the same as for the resonator coils. For case C, covering most of the Smith chart can be achieved with a reasonable inductance range, whereas for case A, the inductance range is not large enough to match all the load impedances.

The limitation discussed above also gives a better understanding of the parasitic effects in the lossy WPT systems. For capacitive method, it is crucial to avoid parasitic capacitances of resonator coils at high frequencies since they are comparable with 0.5 pF, whereas for low frequency applications they can be ignored.

The matchable areas of the lossless model and the circuit with parasitics are compared in Figure 18. Here, blue/yellow colors correspond to matching network type and solid/hatched patterns of charts represent ideal and lossy scenarios of examination. The figure shows that the circuit with inductive IMN is more sensitive to the loss than capacitive IMN. In case A, the reductions in matchable areas of inductive and capacitive IMNs are comparable. In case B and case C, the reduction is higher for inductive IMN than for capacitive IMN. Case C is least affected by the parasitics due to high operation frequency. It should be noted that a larger parasitic resistance shrinks the matchable region, whereas a smaller parasitic resistance increases it closer to the ideal case.

It is clear that matching networks provide quite different areas of perfectly matchable impedances. However, the comparison in Figures 15 and 16 showed that the methods have comparable power transfer when the networks are optimized for each load.

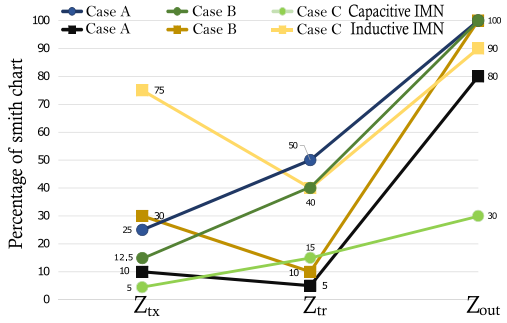

Figure 17. Matchable area comparison for different stages of the circuit in the ideal case.

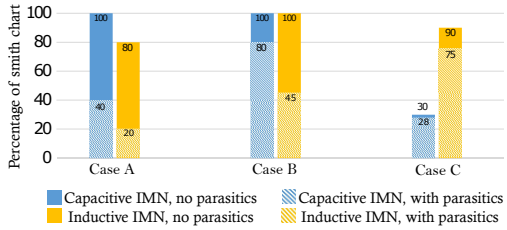

Figure 18. Area of matchable loads before and after introducing the parasitics.

6. Conclusions

In this paper, we compare areas of matchable loads for capacitive and inductive impedance matching networks (IMNs), which are the common matching techniques in the magnetic resonant wireless power transfer system. Graphical visualization of the impedances by Smith Chart is used for effortless comparison of the IMNs performances. An analytic expression for effective output impedance is derived and used to display the conjugate-image impedance of the load. Without any limitations in the parameter values and frequency range, it is always possible to match any load, i.e., any point in the Smith chart. Therefore, three different applications were considered with constraints: case A—car charging operating at 85 kHz, case B—mobile phone charging at 6.78 MHz, and case C—a high-frequency charging device at 100 MHz.

For the lossless system, the capacitive circuit's matchable area fills the Smith chart for case A, whereas around 20% of the chart that cannot be matched by the inductive IMN. For case B both methods could match any load impedance. On the other hand, the inductive IMN has shown about 60% larger area than the capacitive IMN for case C. The matching network at the receiver improves the area in all cases.

Finally, the impact of parasitic resistance of the resonator coils to the matchable area has been examined. In case A, the reduction of matchable area is 60 percentage points for both methods. The matchable area by the inductive IMN is more sensitive to the parasitic resistance than capacitive IMN for cases B and C. However, simulation of power transfer has shown that both matching networks can be equally effective in matching different load values.

Author Contributions: All authors contributed to problem formulation, conceptualization and choice of methods. Y.Z. performed all calculations, simulations and original draft preparation. All authors contributed to interpretation of results, and to editing into the final manuscript. All authors have read and agreed to the published version of the manuscript.

Funding: Y.Z. benefits from a PhD scholarship from University of South-Eastern Norway funded by the Norwegian Ministry of Education and Research. Article processing charge (APC) was funded by the University of South-Eastern Norway.

Acknowledgments: The Research Council of Norway is acknowledged for the support to the Norwegian Ph.D. Network on Nanotechnology for Microsystems, Nano-Network (221860/F40).

Conflicts of Interest: The authors declare no conflict of interest.

References

1. Aqeel, J.M.; Nordin, R.; Gharghan, S.K.; Jawad, H.M.; Ismail, M. Opportunities and Challenges for Near-Field Wireless Power Transfer: A Review. *Energies* **2017**, *10*, 1022. [CrossRef]
2. Akhtar, F.; Rehmani, M.H. Energy replenishment using renewable and traditional energy resources for sustainable wireless sensor networks: A review. *Renew. Sustain. Energy Rev.* **2015**, *45*, 769–784. [CrossRef]
3. Vázquez-Leal, H.; Gallardo, A.; González-Martínez, F.J.; Castañeda-Sheissa, R. *The Phenomenon of Wireless Energy Transfer: Experiments and Philosophy*; INTECH Open Access Publisher: London, UK, 2012.
4. Kurs, A.; Karalis, A.; Moffatt, R.; Joannopoulos, J.D.; Fisher, P.; Soljacic, M. Wireless power transfer via strongly coupled magnetic resonances. *Science* **2007**, *317*, 83–86. [CrossRef] [PubMed]
5. Sample, A.P.; Meyer, D.A.; Smith, J.R. Analysis, experimental results, and range adaptation of magnetically coupled resonators for wireless power transfer. *IEEE Trans. Ind. Electron.* **2011**, *58*, 544–554. [CrossRef]
6. Eplett, B.K. On-Chip Impedance Matching Using a Variable Capacitor. U.S. Patent 2008/0211598 A1, 4 September 2008.
7. Lee, W.; Lee, H.; Oh, K.; Yu, J. Switchable distance-based impedance matching networks for a tunable HF system. *Progr. Electromagn. Res.* **2012**, *128*, 19–34. [CrossRef]
8. Lim, Y.; Tang, H.; Lim, S.; Park, J. An Adaptive Impedance-Matching Network Based on a Novel Capacitor Matrix for Wireless Power Transfer. *IEEE Trans. Power Electron.* **2014**, *29*, 4403–4413. [CrossRef]
9. Kim, J.; Kim D.H.; Park, Y.J. Analysis of Capacitive Impedance Matching Networks for Simultaneous Wireless Power Transfer to Multiple Devices. *IEEE Trans. Ind. Electron.* **2015**, *62*, 2807–2813. [CrossRef]

10. Chen, J. A Study of Loosely Coupled Coils for Wireless Power Transfer. *IEEE Trans. Circuits Syst. II Express Briefs* **2010**, *57*, 536–540. [CrossRef]
11. Kim, J. Coil Design and Shielding Methods for a Magnetic Resonant Wireless Power Transfer System. *Proc. IEEE* **2013**, *101*, 1332–1342. [CrossRef]
12. Kim, J.; Jeong, J. Range-Adaptive Wireless Power Transfer Using Multi-loop and Tunable Matching Techniques. *IEEE Trans. Ind. Electron.* **2015**, *62*, 6233–6241. [CrossRef]
13. Kesler, M. *Highly Resonant Wireless Power Transfer: Safe, Efficient, and Over Distance*; WiTricity Corporation: Watertown, MA, USA, 2013.
14. Hui, S.Y.R.; Zhong, W.; Lee, C.K. A Critical Review of Recent Progress in Mid-Range Wireless Power Transfer. *IEEE Trans. Power Electron.* **2014**, *29*, 4500–4511. [CrossRef]
15. Zhaksylyk, Y.; Azadmehr, M. Comparative Analysis of Inductive and Capacitive feeding of Magnetic Resonance Wireless Power Transfer. In Proceedings of the 2018 IEEE PELS Workshop on Emerging Technologies: Wireless Power Transfer (Wow), Montréal, QC, Canada, 3–7 June 2018.
16. Li, Y.; Dong, W.; Yang, Q.; Zhao, J.; Liu, L.; Feng, S. An Automatic Impedance Matching Method Based on the Feedforward-Backpropagation Neural Network for a WPT System. *IEEE Trans. Ind. Electron.* **2019**, *66*, 3963–3972. [CrossRef]
17. Roberts, S. Conjugate-Image Impedances. *Proc. IRE* **1946**, *34*, 198–204. [CrossRef]
18. Wang, Q.; Che, W.; Monti, G.; Mongiardo, M.; Dionigi M.; Mastri, F. Conjugate image impedance matching for maximizing the gains of a WPT link. In Proceedings of the 2018 IEEE MTT-S International Wireless Symposium (IWS), Chengdu, China, 6–10 May 2018.
19. Dionigi, M.; Mongiardo, M.; Perfetti, R. Rigorous Network and Full-Wave Electromagnetic Modeling of Wireless Power Transfer Links. *IEEE Trans. Microw. Theory Tech.* **2015**, *63*, 65–75. [CrossRef]
20. Zhou, S.; Chris Mi, C. Multi-Paralleled LCC Reactive Power Compensation Networks and Their Tuning Method for Electric Vehicle Dynamic Wireless Charging. *IEEE Trans. Ind. Electron.* **2016**, *63*, 6546–6556. [CrossRef]
21. Uchida, A.; Shimokawa, S.; Oshima, H. Effect of load dependence of efficiency in a multi-receiver WPT system. In Proceedings of the 2017 IEEE Wireless Power Transfer Conference (WPTC), Taipei, Taiwan, 10–12 May 2017.
22. Gernsback, H. *Lighting lamp by S-W- Radio*; Short Wave & Television: New York, NY, USA, 1937, pp. 166–191.
23. Rhea, R. The Yin-Yang of Matching: Part 1—Basic Matching Concepts. *High Freq. Electron.* **2006**, *5*, 16–25.

© 2020 by the authors. Licensee MDPI, Basel, Switzerland. This article is an open access article distributed under the terms and conditions of the Creative Commons Attribution (CC BY) license (http://creativecommons.org/licenses/by/4.0/).

Article IV

Y. Zhaksylyk, U. Hanke and M. Azadmehr, "Impedance Matching using Interspiraled Coils for Wireless Power Transfer," 2020 IEEE PELS Workshop on Emerging Technologies: Wireless Power Transfer (WoW), 2020, pp. 346-349, doi: 10.1109/WoW47795.2020.9291325.

Article V

Y. Zhaksylyk, U. Hanke, and M. Azadmehr, "Single-side interspiraled inductive impedance matching for Magnetic Resonance Wireless Power Transfer", is submitted to IEEE Transactions on Circuits and Systems I: Regular Papers.

Patent

Y. Zhaksylyk and M. Azadmehr, patent "A Coil structure for impedance matching in a wireless power transfer system", filed

Doctoral dissertation no. 152
2023

—

Inductive impedance matching network for Magnetic Resonant Wireless Power Transmission

Dissertation for the degree of PhD

—

Yelzhas Zhaksylyk

—

ISBN 978-82-7206-737-2 (print)
ISBN 978-82-7206-738-9 (online)

usn.no